TIDAL STREAM RESOURCE CLASSIFICATIONS

A Dissertation
Presented to
The Academic Faculty

by

Shubhneet Singh

In Partial Fulfillment
of the Requirements for the Degree
MASTER OF SCIENCE in the
SCHOOL OF CIVIL AND ENVIRONMENTAL ENGINEERING

Georgia Institute of Technology
MAY 2020

TIDAL STREAM RESOURCE CLASSIFICATIONS

Approved by:

Dr. Kevin Haas, Advisor
School of Civil and Environmental Engineering
Georgia Institute of Technology

Dr. Hermann Fritz
School of Civil and Environmental Engineering
Georgia Institute of Technology

Dr. Vincent Neary
Wind and Water Power Technologies
Sandia National Laboratories

Date Approved: April 24, 2020

To mankind

ACKNOWLEDGMENTS

I wish to thank all the people without whose assistance I could not have marked this major milestone in my life. First of all, I want to express my deepest gratitude to my advisor, Dr. Kevin Haas, for being an inspiration and venerable mentor throughout my journey at Georgia Tech. I also feel grateful to Dr. Hermann Fritz and Dr. Vincent Neary for being on my thesis review committee and providing their valuable feedback. I want to pay my special regards to all the professors who instructed me through the course of my Masters and helped me become technically competent. I will be forever indebted to Georgia Tech for providing the environment which academically and socially groomed me into a proficient Water Resource Engineer and an empathetic human being. I would also like to recognize the assistance of my parents, who have unconditionally supported me throughout my education and have been my anchor in the rough waters.

I also thank the Sandia National Laboratories, a multi-mission laboratory managed and operated by National Technology and Engineering Solutions of Sandia, LLC., a wholly-owned subsidiary of Honeywell International, Inc., for the U.S. Department of Energy's National Nuclear Security Administration, for funding this study under contract DE-NA0003525.

TABLE OF CONTENTS

LIST OF TABLES

LIST OF FIGURES

LIST OF SYMBOLS AND ABBREVIATIONS

DOE	U.S. Department of Energy
kW	kilowatts
kWh	kilowatt-hour
LCOE	Levelized cost of energy
MHK	Marine Hydrokinetic
FERC	Federal Energy Regulatory Commission
MW	Megawatt
TPD	Tidal power density
KHPS	Kinetic Hydropower System
R	Pearson’s coefficient of correlation

SUMMARY

Increasing energy demands and rapid climate change warrant the exploration of clean and renewable energy sources. While we have a plethora of renewable energy source options, tidal streams offer a bountiful, reliable, and predictable source of dense and low-carbon energy. As the tidal industry is still in its infancy, the current cost of tidal stream energy production is very high as compared to other non-conventional resources. In this study, a classification system is developed for tidal stream resources available across the U.S., which would assist in preliminary project siting and streamlining the development of tidal energy harnessing devices, which in turn is an effort to make the tidal energy harnessing economically viable. The classification system for tidal energy resource appraisal is based on evaluating the opportunity for energy generation quantified by power and constrained by secondary parameters such as the cross-sectional area and depth of the channel. Further, several relationships are established between the primary classification parameter and other design parameters such as the one-percent exceedance velocity and the maximum velocity at a site to simplify the tidal project development, as it enables the determination of design parameters from the fundamental classification parameters, bypassing tedious data processing. The goal of this study is to develop a tidal resource classification system based on the most important metrics that characterize the resource attributes and the range of values observed for these metrics.

CHAPTER 1. INTRODUCTION

With the rapid growth of population and advancement in technology, we are observing an unprecedented surge in demand for energy. The U.S. Energy Information Administration (EIA) projects nearly 50% surge in the energy demand by 2050. Keeping in mind the current dependence on conventional non-renewable sources (Figure 1) and its environmental repercussions, it is imperative to explore clean, renewable sources to cater the future demands. It is encouraging to see the emerging federal support, increasing investment, and development of technologies in the renewable energy sector, but there is a tremendous scope in the domain as we utilize only 11% of renewable energy in the total annual energy consumption of U.S.

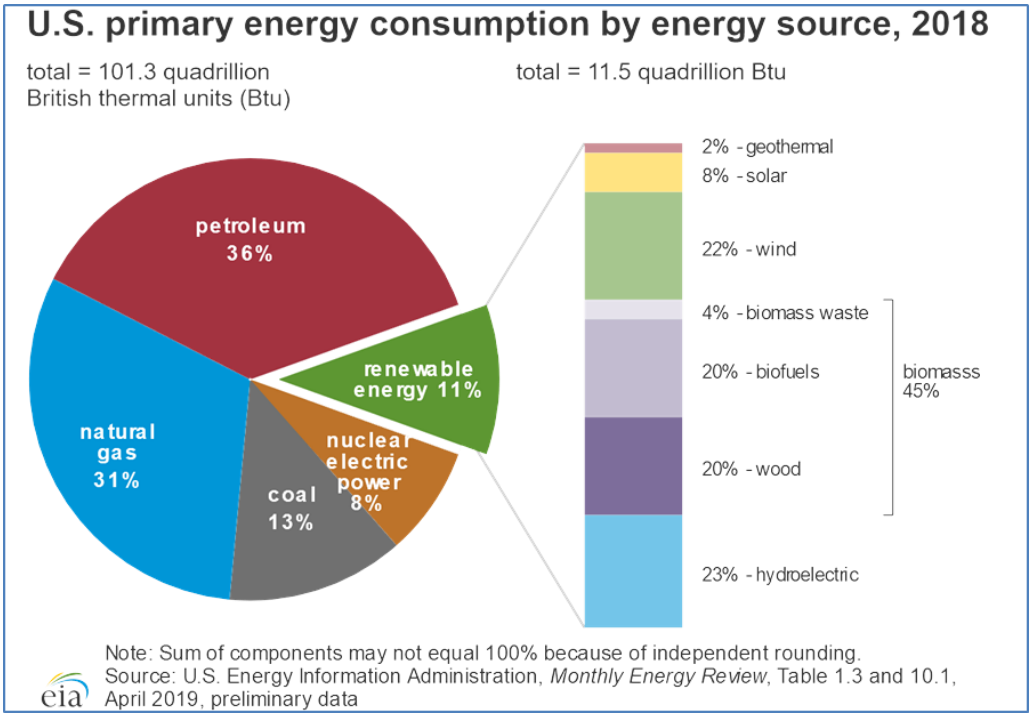

Figure 1 U.S. primary energy consumption by energy source, 2018 (U.S Energy Information Administration, 2019).

The rise in mean global temperature, warming of the ocean, shrinking ice sheets, decreasing snow cover, sea-level rise, ocean acidification, and several extreme weather events are strongly exhibiting the havoc caused on the environment by the increase in greenhouse gases. The rapid increase of greenhouse gases is causing more droughts, heat waves, hurricanes, and changes in precipitation patterns. Global sea level has risen by eight inches since 1880, and it is forecasted to rise by 1-4 feet by 2100. The Earth's average surface temperature has risen by 1.62 F, driven by carbon dioxide emissions since the late 19th century (NASA, 2019). As the evidence is compelling, it is crucial to develop clean energy sources that do not exacerbate the already deplorable condition of the atmosphere. Sustainable development is also one of the underlying motivations to develop renewable energy resources, such as tidal stream energy.

While we have a plethora of renewable energy options, tidal streams offer a bountiful, reliable, and predictable source of dense and low-carbon energy. Its high predictability in comparison to offshore wind and wave energy makes it a promising choice for development. The close alliteration of the word tide and the Anglo-Saxon words tid, time (in modern German) testifies to an early awareness of the tide's regularity and predictability to coastal people. In earlier times, coastal people used the observation of tidal variation as a proxy for time, since it is a clockwork.

There are also additional benefits associated with offshore ocean energy harnessing projects. Coastal energy harnessing farms have also been studied for their advantages of storm-induced coastal flooding prevention under three sea-level rise scenarios: present situation, optimistic projection, and pessimistic projection. The Delft3D-Wave and XBeach-G models have been jointly applied to a gravel-dominated coast in southern Spain.

The results showed that the wave farm induces reductions, for all the three scenarios, in breaking wave heights by about 10% and 25% under westerly and easterly storms, respectively, and total run-up values by 8% and 10%, respectively. Hence, offshore energy projects lead to a reduction in flooded cross-shore distances and dry beach areas (Bergillos et al., 2020).

The extent of the abundant renewable energy possessed by the oceans is commensurate to their expansive surface cover on the earth. The Electric Power Research Institute (EPRI) estimates that the total magnitude of the recoverable wave resource is approximately 1,170 Terra-Watt hours per year, while the combined ocean current, ocean tide, and U.S. river resource are about 500 Terra-Watt hours per year. Combined, the total MHK resource is nearly 1/3 of the U.S. electricity demand of roughly 4,000 Terra-Watt hours per year (Jenne et al., 2015).

In 2019 the US EIA published figures for the average levelized cost of energy per unit of output (LCOE) for generating technologies to be brought online in 2023, as modeled for its Annual Energy Outlook. The reported LCOE for various energy sectors are - advanced nuclear, 77.5 $/MWh; coal with 90% carbon sequestration, 98.6 $/MWh (rising to 104.3 $/MWh at 30%). Among the non-dispatchable technologies, LCOE estimates vary widely: from 49.8 $/MWh for wind onshore, 45.7 $/MWh for solar PV, 117.5 $/MWh for offshore wind, to 121.2 $/MWh for solar thermal (EIA, 2019). However, for tidal current turbines, the LCOE is $1990/MWh and $400/MWh for 1-unit and 10-unit array deployment (Jenne et al., 2015). The current cost of tidal stream energy production is prohibitively high as compared to other non-conventional resources.

As the tidal industry is still in its infancy, and only a few stream energy conversion projects have been implemented at the pre-commercial demonstration stage in the United States. Verdant Power operated a grid-connected demonstration array of six Kinetic Hydropower System (KHPS) turbines, a three-bladed horizontal-axis turbine at the RITE Project site in the East Channel of the East River, referred to as the RITE Demonstration. In December 2006, the first grid connected KHPS turbine was installed, followed by the other five turbines in 2007. The successful RITE demonstration is the world's first grid-connected array of tidal turbines (Verdant Power, 2019).

In many parts of the world, the tidal power sector is consolidating, under planning and in testing phases. United Kingdom is successfully operating projects like MeyGen and Shetland Tidal Array. MeyGen Tidal Energy Project, at the Inner Sound of the Pentland Firth, completed its construction phase and started its 25-year operational phase in April 2018. MeyGen has exported more than 15 GWh of tidal energy to the grid in Scotland as of May 2019 (MeyGen, 2020). Shetland Tidal Array, located in the Bluemull Sound, has three turbines of 100 kW capacity each. Nova Innovation is the lead partner in the development of Shetland Tidal Array, and it has been awarded €5 million funding for another Horizon 2020 project, ELEMENT, which will incorporate Artificial Intelligence technology to improve tidal turbine performance (Shetland Tidal Array, 2020).

There are few other sites in Canada and United Kingdom, where the pilot studies have been conducted and the projects are still under development. At Race Rocks, offshore of Vancouver Island in British Columbia, Canada, a 65-kW tidal turbine generator was successfully installed and tested to extract power in flows exceeding 3.5 m/s (Race Rocks, 2020). SeaGen, is another device tested in the Strangford Narrows, Northern Ireland. It is

1.2 MW device that was installed by Marine Current Turbines and commenced operation in 2009 to collect data to influence future turbine design and environmental impact, in particular on marine animals (Strangford Narrows, 2020).

Some projects are under the planning phase at promising locations like Clarence Strait in Australia, Gulf of Kutch in India, Island of Alderney in United Kingdom (Alderney, 2020; HydroReview, 2020; Clarence Strait, 2020).

The increase in energy demand and deteriorating climate change have thrusted the exploration of renewable energy, recent development in sustainable energy sources has rekindled the interest in marine and hydrokinetic (MHK) resources. Also, federal production and tax-credits are leading to the rapid evolution of MHK technologies. This growing interest is reflected by the number of license requests submitted to the Federal Energy Regulatory Commission (FERC). As of December 2012, FERC had issued four licenses and 84 preliminary permits, while an additional 42 projects are in the pre-filing stage for a license to install MHK projects (Board, O.S., 2013).

For delving further into tidal stream energy harnessing projects, it is essential to appraise the value of available resources along the U.S coast for converting into electricity. The success of wind resource appraisal and classification systems has motivated interest in similar classification systems for tidal resource potential. A tidal energy resource classification system used to appraise the value of the resource in terms of opportunity for energy capture based on power density would serve as a useful resource assessment tool that facilitates siting, project scoping studies, and regional energy planning (Neary et al. 2019).

In this study, the goal is to develop tidal resource classification schemes for the U.S. to reap similar benefits as the wind industry. Classification parameters calculated for U.S. tidal energy resources using a combination of model hindcast and measurement databases, following the requirements given in technical specifications IEC/TS 62600-200 and IEC/TS 62600-201. For resource classification, the mean annual power density and other resource classification parameters, such as depth, surface area, cross-sectional area are determined from the national tidal resource assessment database (Haas et al., 2011). The large population of values for these potential classification parameters, representing the full range of tidal resource attributes for the US, are evaluated to calculate correlations between them and to identify the basic tidal resource parameters from which other condition parameters can be gleamed. Further, the goal of this study is to develop a tidal resource classification system based on the most important metrics that characterize the resource attributes and the range of values observed for these metrics.

In this document, a brief overview of the motivation for tidal energy exploration, the current status of the energy market, and the goal of the study undertaken is discussed in the introduction. Chapter 2 briefly reviews tidal stream energy assessment across the U.S, the estimation of available theoretical power, types of device used to harness tidal energy, numerical model to simulate the tidal variation, and parallels drawn in the tidal industry from the wind industry. Furthermore, all the data computation of tidal stream data across the U.S coast to define a resource classification system is propounded in Chapter 3. Finally, the conclusions are drawn and the suggestions for augmenting this work are documented in the last chapter.

1.1 Ocean Renewable Energy

In the efforts to explore MHK energy resources, the Department of Energy directed the Energy Policy Act of 2005 to appraise the MHK resource base. The contract was assigned to five assessment groups to conduct an independent study of the extractable energy from five categories of MHK resources: waves, tidal currents, ocean currents, marine temperature gradients, and free-flowing water in rivers and streams (Board, O.S., 2013). The estimates of the potential of all the categories of MHK resources are listed in Table 1.

Table 1 Resource base appraisal of all the MHK energy sources for the U.S. (EE&RE, 2019).

Resource Assessment	Resource Potential
Waves	Theoretical: 1,594–2,640 TWh/year Technical: 898–1,229 TWh/year
Tidal streams	Theoretical: 445 TWh/year Technical: 222–334 TWh/year
Ocean currents	Theoretical: 200 TWh/year Technical: 45–163 TWh/year
River currents	Theoretical: 1,381 TWh/year Technical: 120 TWh/year

Global resources for ocean energy have been estimated to have a net potential higher than that of wind and solar power (about 32,000 GW), and it has the potential to provide up to 7% of the global electricity demand. It is a very promising form of energy due to its immense potential and predictability (EE&RE, 2019).

Ocean renewable energy resource is usually quantified by the theoretical, technical, and practical resource. The theoretical resource is the amount of energy that is present in the natural as potentially available energy. The technical resource is defined as the amount of the theoretical resource that can be technically captured by using the currently available devices. The practical resource is the portion of technical resource further filtered by the environmental, social, and economic constraints (Ahn et al., 2019). Although theoretical MHK resource is abundant, but it is seldom converted into practical resources. Hence, to have a more realistic resource assessment, technical power is a better parameter than theoretical power to appraise the resource for preliminary studies. In the following subsections, various types of MHK resources are discussed further.

1.1.1 Wave Energy

For the US, according to the Electric Power Research Institute and U.S Department of Energy, the total theoretical wave energy resource along the US continental shelf to the notional 100 m depth contour is estimated to be 1851 TWh/year. The technical resource with at least 8 kW/m is 899 TWh/year, representing 22.2% of the 2012 US Annual Energy Production (AEP) and the maximum practical resource is 522 TWh/year, representing 12.9% of the 2012 US AEP. The theoretical resource in some regions of the US is substantial, with estimates at 502 TWh/year on the West Coast (CA, OR, WA), 973 TWh/year in Alaska, 98 TWh/year in Hawaii representing over 100% of the regional

2012 AEP (Ahn et al., 2019). The geographical distribution of the total wave power along the US coastline is shown in Figure 2.

Also, in Europe, the wave energy sector is a relatively small but valuable contributor

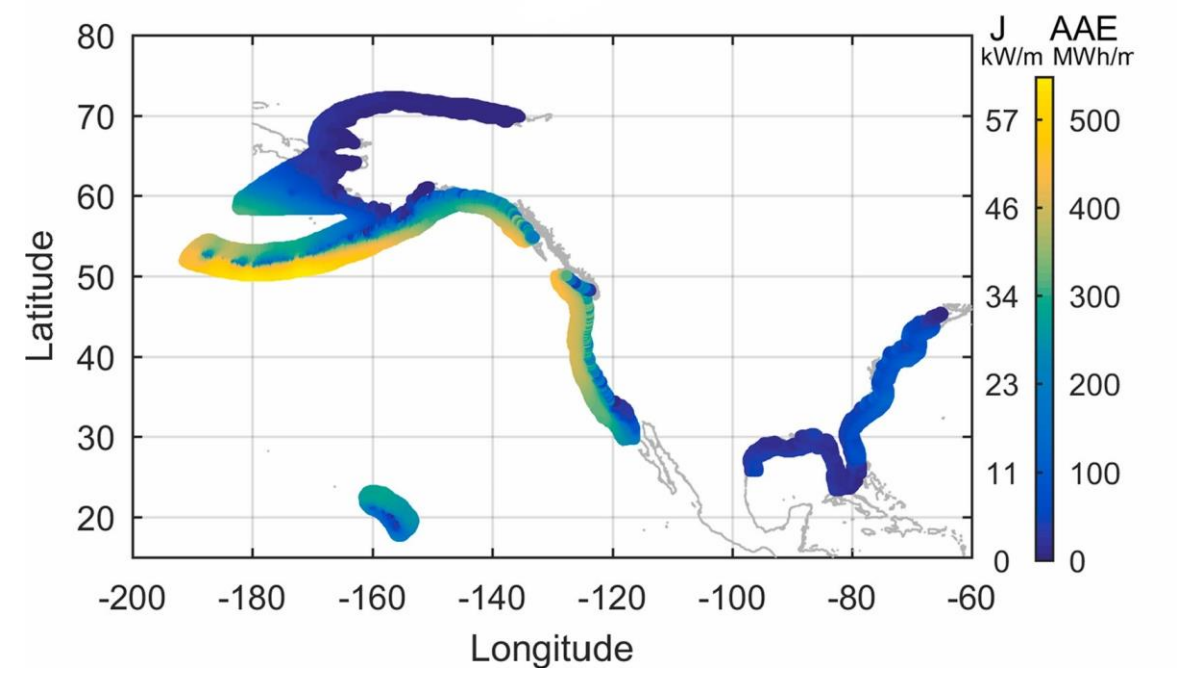

Figure 2 The geographical distribution of the total wave power along the US coastline (Ahn et. al., 2019).

to the renewable energy mix. The EU's wind energy capacity currently covers 7.6% of the EU's electricity needs (Eurostat, 2013). By comparison, deploying 500,000 wave energy devices in Europe would produce up to 45 GW of energy per year, which would cover 12% of Europe's current electricity consumption (Schlütter et al., 2015).

1.1.2 Tidal Stream Energy

Generally, tidal stream power devices require a minimum flow speed (cut-in speed) to start operating, which ranges from 0.5 m/s to 1 m/s depending on the design (Defne et al., 2012). The tidal devices also have a minimum depth constraint to allow enough top and

bottom clearance. In this study, all the sites across the U.S coast with the velocity less than 0.5 m/s and locations with depth less than 5m were filtered out.

An extensive study to assess the national tidal stream resource was undertaken by Defne et al., 2012. They have identified all the sites with a maximum of the average kinetic power density greater than 500 W/m^2, a surface area larger than 0.5 km^2, and depth larger than 5 m as hotspots.

Defne et al., 2012 estimated the annual maximum theoretical power available at all the identified hotspots across the U.S. coast as 50,783 MW. A significant chunk of the total tidal energy is found to be in Alaska, which is followed by Maine, Washington, Oregon, California, New Hampshire, Massachusetts, New York, New Jersey, North and South Carolina, Georgia, and Florida. The average tidal stream power density at some of these locations is larger than 8 kW/m^2 with surface areas on the order of a few hundred kilometers squared and depths greater than 100 m. Cook Inlet, Alaska is distinguished relative to the other hotspots with a sizeable tidal stream power density sustained over an extraordinarily large area.

1.1.3 Ocean Current Energy

The world's oceans cover more than 70% of the earth's surface and are a promising reservoir of alternative energy resources. The general ocean circulation is characterized by large rotating ocean gyres resulting in rapid ocean currents along the western boundaries in the northern hemisphere because of the Coriolis Effect. Energy production from the ocean presently constitutes a negligible portion of our daily energy supply, while the

worldwide electricity produced by ocean-based devices is predicted to reach more than 7% by 2050 (Yang et al., 2015).

The Gulf Stream system is formed by the western boundary current of the North Atlantic Ocean flowing along the east coast of the United States and is of interest as a potential energy resource for the United States. Beginning in the Caribbean and ending in the northern North Atlantic, the Gulf Stream is one of the world's most intensely studied ocean current systems. On average, the Gulf Stream is approximately 90 km wide and 1000 m deep. The current speed is fastest near the surface, with the maximum speed typically exceeding 2 m/s. The available power of approximately 5 GW associated with the undisturbed natural flow condition from the Gulf Stream system is predicted based on hypothetical turbine parameters. (Yang et al., 2015).

1.1.4 Riverine Hydrokinetic Energy

The theoretical riverine hydrokinetic energy, aggregated for the contiguous lower 48 states, is estimated at 1,146 TWh/yr. The aggregate estimate of the Alaska theoretical resource is 235 TWh/yr, yielding a total theoretical resource estimate of 1,381 TWh/yr for the continental US. The Lower Mississippi region contributes nearly half (47.9%) of the total resource estimate. The major rivers of Alaska constitute 17.1% of the total for the continental U.S. The next most significant contributor is the Pacific Northwest region, which contributes 9.2%, followed by the Ohio region (5.7%). Collectively these four regions encompass 80% of the technically recoverable hydrokinetic resource in the continental U.S. (Jacobson et al., 2012).

CHAPTER 2. LITERATURE REVIEW

Tidal power is the form of hydrokinetic energy which can be harnessed from the tidal currents in the coastal region, due to the fall and rise of the sea level caused by the gravitational pull of the sun, moon, and the rotation of the Earth. These currents are enhanced at the places where the bathymetry constricts the flow through a narrow passage. The currents flow reverses its flow direction with the rising and falling of water elevation. The current directed toward the shore is called the flood current, and the current flowing away from the coast is called ebb current. The time duration, when the current is zero, during the switching of the current direction, is called the slack period. These tidal variations, both the rise and fall of the tide and the flood and ebb currents, can be utilized to generate electricity. The regular and highly predictable nature of the astronomically driven tidal cycles makes it an excellent source of renewable energy compared to other less predictable non-conventional sources like wind and ocean waves energy.

2.1 Tidal stream energy assessment and hotspots along the U.S. coast

The tidal stream power is estimated by evaluating the kinetic power density (P) at a particular location by using the

$$P = \frac{1}{2} . \rho . V^3 \tag{1}$$

where P is the tidal stream power per unit area of flow, i.e., tidal stream power density, ρ is the density of seawater, and V is the current speed. For the tidal stream resource

harnessed using the tidal devices, power density is a suitable parameter to filter the hotspot locations, as most of the tidal devices have a minimum current speed for operating. Assessing the extractable power, which includes the kinetic and potential energy, requires a more rigorous estimation method, which accounts for the backwater effect due to the presence of tidal devices in the stream, which is discussed in the next section. Although, for preliminary site screening and identifying the hotspots, the sites can be filtered based on current velocity and the available depth.

In previous studies by Defne et al., 2012 and Kilcher et al., 2016, the hotspots have been defined by the minimum value of the power density as 500 W/m^2. Regardless of the device design, the tidal stream power converters also require a minimum depth that allows for accommodation of the device with enough top and bottom clearance. The dimensions of tidal stream power devices change from several meters to tens of meters (Bedard et al., 2006; Froberg, 2006), and since the analysis in this study does not depend on a specific device, the minimum depth is chosen to be 5 m, large enough to accommodate a small size conversion device with the existing technology. The list of hotspots is also filtered with a minimum surface area requirement of 0.5 km^2 (Defne et al., 2012).

The list of hotspots considered for this study (Appendix A) is inclusive of all the hotspots identified by Defne et al., 2012, and Kilcher et al., 2016. It can be observed that Alaska (AK) has the largest number of hotspots, including some of the most significant kinetic power densities in the USA, with a surface area that is an order of magnitude larger than the rest of the hotspots. Tacoma Narrows, Western Passage, Rosario Strait, Cook Inlet, are considered as the top 4 ranked hotspots to tap tidal stream power in the U.S. (Kilcher et al., 2016). The largest kinetic power density locations include Bristol Bay, Akutan,

Unalga and Samalga Passes, Sikitnak Island, Turnagain Arm, and Kopreanof, Icy, and Peril Straits. Maine (ME), Washington (WA), Oregon (OR), California (CA), New Hampshire (NH), Massachusetts (MA), New York (NY), New Jersey (NJ) North and South Carolina (NC, SC), Georgia (GA), and Florida (FL) follow Alaska in the total amount of tidal resource availability by state (Defne et al., 2012).

2.2 Total theoretical available power estimates

The national tidal resource database provides the distribution of the existing kinetic power density of tidal streams in the undisturbed flow conditions across the U.S. coast. However, these results do not include any technology assumptions or flow field effects, as in the case of device arrays. In order to calculate a theoretical upper bound based on physics only, a simplified method that considers both the kinetic and potential power with the exclusion of any technology, specific assumptions are applied. Maximum theoretical power available, P_{max} is given to a reasonable approximation by:

$$P_{max} = 0.22 g \rho a Q_{max} \quad (2)$$

where g is gravity, a is the tidal amplitude (the height of high tide above mean sea level), and Q_{max} is the maximum volume flux into a bay in the natural state without turbines. The details of the method are outlined in a paper by Garrett and Cummins, 2005.

In the P_{max} scenario, the fence of turbines is effectively acting as a barrage, so that P_{max} is essentially the power available when all water entering a bay is forced to flow through the turbines. P_{max} is thus likely to be a considerable overestimate of the practical

extractable resource once other considerations, such as the extraction and socioeconomic filters, are considered (Board, O.S., 2013).

The power calculated with this method is used in estimating the tidal power potential for the entire country broken down for each state. The technique uses the undisturbed flow field from the model with simple analytical methods, accounts for the cumulative effect of dissipating energy, and provides information on an estuary scale (Defne et al., 2012).

In a search for suitable parameters for tidal resource classification in this study, the secondary parameter is needed, such that it acts as a proxy for the amount of extractable energy at a site and eliminates the need for the tedious computation of maximum theoretical power.

Similar to resource assessment based on kinetic energy, Alaska has the largest contribution of 47 GW to the national total. Cook Inlet has the largest average maximum available power of 18 GW closely followed by Chatham Strait with 12 GW. Alaska stands out as an abundant resource of the tidal stream with 80 different hotspots (Defne et al., 2012).

However, the assessment of the upper bound for power conversion from tidal currents at these hotspots requires a more detailed study as the overall power that can be converted from tidal streams is also a function of environmental constraints. The environmental constraints include complex issues. For example, conflicts with existing uses, such as shipping and commercial fishing; performance of power converters in high suspended sediment and seasonal sea ice environments; changes to hydrodynamics and sediment transport and alterations to marine habitat and benthos, which are difficult to

quantify due to knowledge gaps and a lack of clear monitoring protocols (Defne et al., 2012).

2.3 Devices to harness tidal energy

The conventional way to harness energy from the water level variation on the coast due to tides is by building up a dam-like structure, called barrage (Figure 3), to raise the water head and to use that potential energy of the water stored to convert into electricity. The barrage is installed across an inlet of an ocean bay or lagoon that forms a tidal basin. Sluice gates on the barrage control water levels and flow rates to allow the tidal basin to fill on the incoming high tides and to empty through an electricity turbine system on the outgoing ebb tide. A two-way tidal power system generates electricity from both the incoming and outgoing tides (U.S. EIA, 2019).

Figure 3 Barrage of the tidal power plant on the estuary of the Rance River in Bretagne, France (U.S. EIA, 2019).

There are only 40 sites known in the world that have the required difference in water levels between tides needed to produce electricity (U.S. EIA, 2019). Tidal barrages have also been linked with the loss of intertidal habitat, increased risk of eutrophication. Installation of tidal barrage also alters the tidal water elevation in the basin and increases the turbidity of the water and poses an obstruction to migratory fishes and navigation across the waterway (Hooper et al., 2013).

Several tidal barrages are operating in China, South Korea, Russia. The Sihwa Lake Tidal Power Station in South Korea has the largest electricity generation capacity at 254 megawatts (MW). The oldest and second-largest operating tidal power plant is in La Rance, France, with 240 MW of electricity generation capacity. The next largest tidal power plant is in Annapolis Royal in Nova Scotia, Canada, with 20 MW of electricity generation capacity. The United States does not have any tidal power plants, and it only has a few sites where tidal energy could be economical to produce using the conventional barrage system. France, England, Canada, and Russia have much more potential to use tidal power (U.S. EIA, 2019).

In recent years exploration has been done to harness the tidal energy by deploying the in-stream turbines in the tidal currents instead of the conventional barrage system. By way of scale comparison, a current velocity is equivalent to a hydraulic head of $0.5v^2/\mathrm{g}$ (where g is gravity), so that even a strong current of 3 m/s (~10 ft/s) is equivalent to a hydraulic head of only 0.5 m (~1.6 ft), which is considerably less head than a typical tidal range. As the power produced by turbines is a function of both, hydraulic head and the current speed, capturing the energy by in-stream devices is relatively speaking not as efficient as capturing channelize energy from the potential head in barrage systems. It is

often claimed that in-stream turbines have less serious ecosystem impacts than barrages, though it is not clear that this is true for installations with the same average power output. In spite of these reservations, and because in-stream turbines could possibly be used in small-scale projects or areas without a large tidal range, much work has gone into evaluating their potential (O.S. Board, 2013).

Extracting energy from the tidal currents, conceptually, is analogous to wind energy. Tidal turbines produce the energy, propelled by the tidal currents underwater, just as the wind turbine does it over the land using wind. Hydrokinetic turbines have some advantages over the conventional barrages; they are significantly smaller in scale than tidal barrages, requiring much lower capital expenditures. Also, they are typically deployed in distributed arrays with many individual units, much like wind farms, minimizing maintenance-related downtime on overall power production (Haas and Muscalus, 2018).

The vast majority of turbines utilize rotors for converting the kinetic energy of the flow into mechanical energy; however, there are examples of turbines using other means such as an oscillating hydrofoil. A wide variety of classification systems of tidal turbine technology have been proposed. A database of all existing tidal technology compiled by the US Department of Energy uses three main categories: axial flow, cross-flow, and reciprocating (Haas and Muscalus, 2018).

A present lack of consensus among tidal energy technologies, including components and subcomponents, constitutes a further obstacle that the sector needs to overcome because this makes it more expensive and unreliable when compared to other renewable technologies. The international nomenclature has defined a classification based on this sort

of conversion of tidal energy into mechanical energy, and distinguishes the following categories (Segura et al., 2018):

(i) Horizontal axis devices with parallel axis to the flow (Figure 4a).

(ii) Vertical axis devices (Figure 4b).

(iii) Horizontal axis devices with a perpendicular axis to the current (Figure 4c).

(iv) Oscillating hydrofoil (Figure 4d).

(v) Other devices (helical screw (Figure 4e) and tidal kite (Figure 4f).

A different classification can be defined based on the depth of the water column (Segura et al., 2018):

(i) First-generation devices that operate at depths of up to 40 m (Figure 5a–c), although some authors indicate depths of between 25 and 50 m with peak flows over 2.5 m/s.

(ii) Second generation devices that the device itself is able to float and can be joined to the seabed via mooring lines or anchoring lines (Fig. 5d).

(iii) Third generation devices that include those devices that can harness energy from small velocity streams (see Figure 4f).

Figure 4 Typical TEC for marine current harnessing: (a) Horizontal axis device with parallel axis to the flow; (b) Vertical axis device (Kobold turbine); (c) Horizontal axis device with perpendicular axis to the flow; (d) Oscillating hydrofoil; (e) Helical screw and; (f) Tidal kite (Segura et al., 2018).

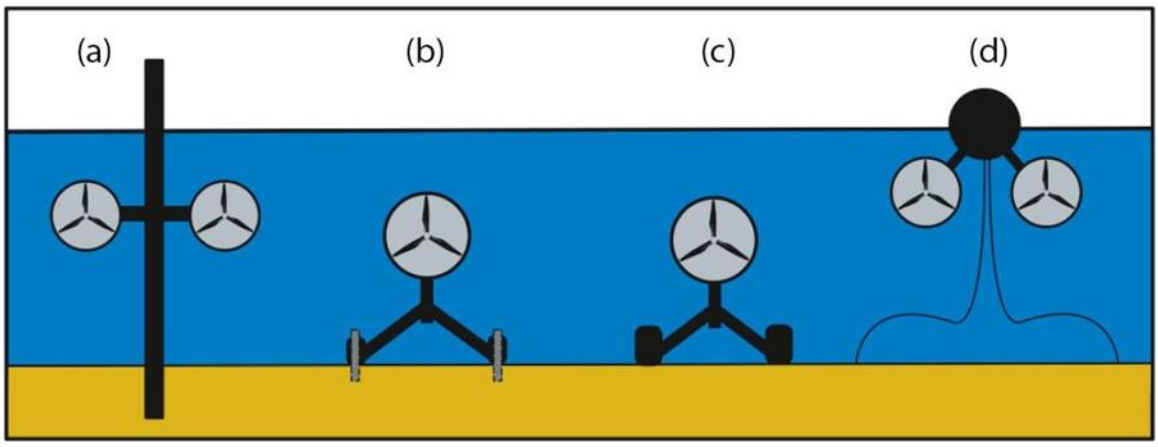

Figure 5 TEC foundation types: (a) Monopile; (b) Piloted; (c) Gravity and; (d) Floating (Segura et al., 2018).

Another aspect is that these designs have, until now, been developed by small companies, many of which have been spin-offs of university projects. Several large technical developers such as ABB, Alstom, Andritz, Siemens or Voith Hydro, among others, have recently entered this emerging sector by becoming involved in the start-up phase and creating the conditions necessary to scale up the existing full-scale demonstration turbines into arrays (these projects, owing to the high operating and development costs, are usually unviable for small and medium companies) (O.E.S., 2016). Furthermore, companies like General Electric have shown great interest and are supplying electrical power systems for some of the prototypes (Segura et al., 2018).

2.4 United States wind energy classification system

In the 1970s, a preliminary wind resource assessment of the United States was carried out that produced 12 regional wind energy maps (Manwell et al. 2010). The atlases depicted the annual and seasonal wind resources on state and regional levels. They also included the wind resource's certainty rating (an indication of the reliability of the data)

and an estimate for the percentage of land suitable for wind energy development based on variations in land-surface form. These data were used to produce a general wind power potential map that gave an indication of the wind resource (in W/m^2) for all locations in the United States in one map. But quite soon, the drawback of the resource mapping was realized. An intensive program was therefore initiated by the Pacific Northwest Laboratories (PNL) to better characterize the wind energy potential in the United States. This led to a publication of a new resource atlas in 1987, which integrated the previous wind measurements with topography and landform characteristics to appraise the wind resource of U.S. The updated wind resource values are depicted on gridded maps, latitude by 1/3 longitude resolution (about 120 km^2), on both a national scale and a state-by-state basis. In the 1987 atlas, the magnitude of the wind resource was expressed in terms of seven wind power classes, rather than as a function of wind speed (Manwell et al. 2010). The wind power classes range from Class 1 (for winds containing the least energy) to Class 7 (for winds containing the most energy). Each class represents a range of mean power density (W/m^2) or equivalent mean wind speed at specified heights above the ground. Table 2 shows the wind power classes in terms of their mean wind power density and the mean wind speed at 50 m above the ground. Finally, the wind resource is mapped based on the classification scheme across the U.S in Figure 6 (Manwell et al. 2010).

A review of wind classification systems indicates two distinct systems, one to appraise the wind resource, and one to appraise the wind condition (power) class for use in the device design standard. The US wind resource classification system, shown in Table 2, was designed to appraise the resource potential as measured by the wind power density at

50 m. This resource classification system has supported project siting and numerous project scoping and regional energy planning studies (Neary et al., 2018).

Table 2 The US wind resource classification system. Seven classes appraised solely on resource potential based on wind power density. Note that classes are spaced every 100 W/m^2 from Class 2 (marginal) to Class 5 (excellent) (Neary et al., 2018).

Wind Power Classification

Wind Power Class	Resource Potential	Wind Power Density at 50 m W/m^2	Wind Speed[a] at 50 m m/s	Wind Speed[a] at 50 m mph
1	Poor	0 - 200	0.0 - 6.0	0.0 - 13.4
2	Marginal	200 - 300	6.0 - 6.8	13.4 - 15.2
3	Fair	300 - 400	6.8 - 7.5	15.2 - 16.8
4	Good	400 - 500	7.5 - 8.1	16.8 - 18.1
5	Excellent	500 - 600	8.1 - 8.6	18.1 - 19.3
6	Outstanding	600 - 800	8.6 - 9.5	19.3 - 21.3
7	Superb	> 800	> 9.5	> 21.3

[a] Wind speeds are based on a Weibull k of 2.4 at 500 m elevation.

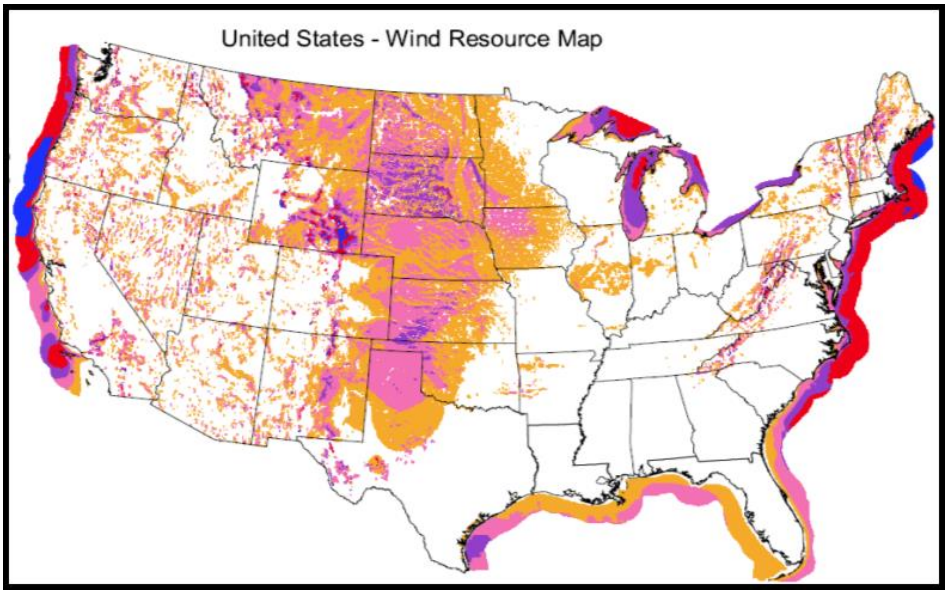

Figure 6 Geographic distribution of wind resource classes across the U.S. based on the class color code defined in table 2.

2.5 Recent developments in tidal stream energy

In the past years, several prototype turbines have been developed, but tidal turbine technology, being relatively new sector, has not yet reached convergence (as opposed to wind turbine technology, which has converged on a three-blade, horizontal-axis design) (Board, O.S., 2013).

In the United States, there have been multiple tidal turbine pilot projects undertaken, including the Verdant project in the East River in New York, the Snohomish Public Utility project in Admiralty Inlet, Washington, and the Ocean Renewable Power Company (ORPC) project in Cobscook Bay, Maine. These projects demonstrate the variety of technology and the scales of tidal power generation.

Verdant Power's Roosevelt Island Tidal Energy (RITE) Project is located in the east channel of the East River, which is a tidal strait connecting the Long Island Sound with the Atlantic Ocean in the New York Harbor. Verdant Power has conducted prototype and pre-commercial testing of its Free Flow System at the RITE Project, as well as groundbreaking regulatory and environmental monitoring that has advanced the US marine energy industry. The demonstration included the operation of six full-scale tidal turbines (Figure 7), which delivered electricity to operating New York City businesses, representing the world's first operation of a grid-connected array of tidal turbines (Verdant Power, 2019).

A Phase II demonstration (RITE demonstration) of the Verdant technology (Kinetic Hydropower System – KHPS) in 2006-08 at the Roosevelt Island Tidal Energy (RITE) Project in the East River showed that the observed turbine peak efficiency of 38 to 44% was as expected in water current speeds of three to seven feet/sec while delivering

emission-free, renewable electricity to two commercial end-users located on Roosevelt Island (Verdant Power, 2011).

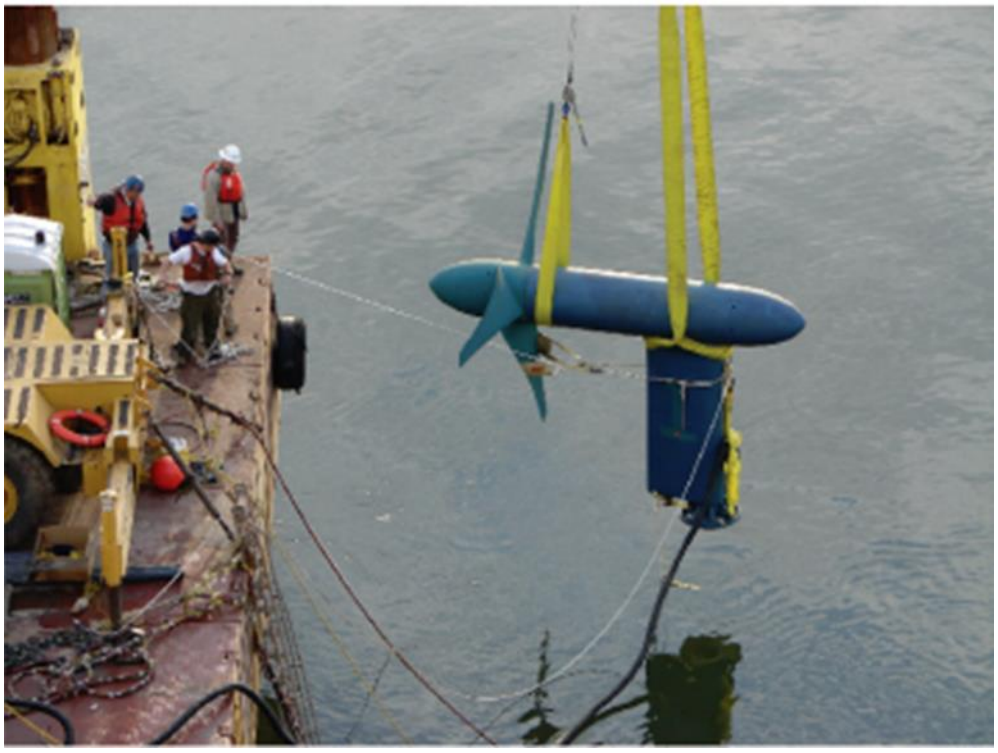

Figure 7 Three-blade hydrokinetic generators on the New York City's East River for Verdant Power's Roosevelt Island Tidal Energy Project (U.S. EIA, 2019).

In Cobscook Bay, Ocean Renewable Power Company (ORPC) installed five 30-m-long ORPC designed with the total generation capacity of up to 300 kW. ORPC designed the TidGen® Power System turbines with a crossflow helical design to operate in water depths of 60 to 150 ft. The Project began delivering electricity to the Emera Maine grid in September 2012, but the TidGen® was retrieved from the Cobscook Bay tidal energy project site in July 2013. After the successful testing phase, U.S. Senators Susan Collins and Angus King announced a grant of $5,350,000 through the Department of Energy (DOE) to enhance the performance of its tidal turbine system on August 31, 2016. While

the project site serves as an excellent testing area, ORPC considers the tidal current velocities at the Project site inadequate to justify pursuing a commercial license. In a March 14, 2017 submittal to FERC, ORPC stated that it did not intend to file a notice of intent or Pre-Application Document (PAD) for the Project (LLC, O.M., 2014).

Within Admiralty Inlet, two 6-m diameter open-center turbines designed by OpenHydro turbines with a nominal output of 150 kW of generation each, using a ducted horizontal-axis design with fixed pitch and yaw, were to be installed. But, on September 30, 2014, Snohomish Public Utility District (PUD) announced that the projects would no longer advance, stating that the US Department of Energy decided not to share the rising costs of the next stage of development. According to the PUD, the requirements became more onerous than expected for a temporary research project (Tethys, 2019).

As of December 2019, three Hydrokinetic, tidal project licenses (Table 3) have been issued by the Department of Energy, U.S. (FERC, 2019).

Table 3 Current Licenses issued by DoE (FERC, 2019).

Project No.	Project Name	Expiration Date	Issue Date	Authorized Capacity (MW)	Licensee	Waterway	State	Description
P-12611	Roosevelt Island	12/31/22	01/23/12	1.050	Verdant Power, LLC	East River, NY	NY	HydroKinetic-Tidal
P-12711	Cobscook Bay	01/31/20	02/27/12	0.300	ORPC Maine, LLC	Cobscook Bay, Atlantic Ocean	ME	HydroKinetic-Tidal
P-13511	Igiugig	04/30/29	05/23/19	0.07	Igiugig Village Council	Kvichak River	AK	HydroKinetic-Inland

CHAPTER 3. TIDAL STREAM CLASSIFICATION

Classification is the process of identifying and categorizing something based on shared characteristics. Classification of the energy characteristics for tidal streams across the U.S. coast would enable us to identify the sites with availability and scalability of tidal energy for harnessing. The success of the wind energy classification system has motivated interest in developing the analogous classification system for tidal stream energy (Haas et al., 2019).

Like wind industry standards, the primary resource classification of tidal stream energy is fundamentally based on the power density, but to appraise the scale of energy available, an additional parameter is essential to define additional stream constraints (e.g., cross-sectional area and/or depth). Hence, the tidal resource classification system is designed to appraise the value of available energy, based on the power density, and the scale of energy available based on a secondary parameter. Various physical parameters of the resource are considered for the secondary parameter in this study, like cross-sectional area, depth, width, and surface area.

The resource classification system would serve as an assessment tool in project siting, scoping studies, and regional energy planning. This work could be augmented by developing a separate device classification system, by establishing standard classes for limiting environmental conditions for device design that would streamline development and manufacturing, while minimizing technical and financial risks for investors.

The vision is for such a system to be incorporated within IEC/TS 62600-201 tidal energy resource assessment standards, focusing mainly on feasibility assessments. (Neary et al., 2018).

3.1 Motivation

The tidal energy classification scheme would address the following core challenges identified by The Office of Energy Efficiency & Renewable Energy's (EERE) marine energy program (Water Power Program, 2019):

1) Marine and Hydrokinetic Energy (MHK) resources have a broad range of intensities, which present difficulties for designing efficient device systems to harness energy.

2) Performance metrics are not well established to evaluate the full range of existing technologies for early-stage project planning.

3) Many high-value opportunities for utilizing MHK technologies are unclear in the electric sector.

3.2 Candidate classification parameters

The primary resource classification parameter, mean annual power density, is calculated from the yearly tidal current time series. Juxtapose to wind energy; the tidal flows are depth-and width-limited, these are additional resource quantification constraints which are addressed by considering a secondary parameter for classifications. For the tidal condition classification parameter, various other parameters can also be considered, like

the mean current speed, which characterizes the normal tidal condition, 1 percent exceedance current speed and the maximum current speed, i.e., the perigean spring tidal current speed occurring three to four times a year, characterizes the extreme tidal condition (Neary et al., 2018). For tidal stream classification, the parameters considered are listed in Table 4 below.

Table 4 Various parameters computed and considered for Tidal Energy Classification.

Variable	**Justification**
Mean annual tidal current speed (m/s)	It is an important parameter to identify the sites for energy extraction. The yearly mean power density can also be computed from the annual mean velocity at a location.
Maximum current (m/s)	The measure of extreme tidal condition, and candidate for TEC classification (to categorize device classes) parameter.
Depth (m)	It was considered for a secondary parameterization, as it is a proxy of scalability of energy extraction. Also, there is a depth constraint for optimum performance for many technologies.
Width (m)	The width was also considered as a secondary parameter, as it gives an insight into the scale of an array that could be installed in a stream.

Cross-sectional area (m^2)	As the cross-sectional area is directly proportional to the total volume flux, it could be an excellent proxy for extractable energy.
Surface area (km^2)	The surface area does not contribute to power density but is required to accommodate a larger space for development and could be a proxy for extractable energy.

Another important consideration for the primary classification parameter is the large-scale far-field backwater effect of an array of turbines. In addition to local flow disturbance around an individual turbine, drag associated with the presence of turbines will reduce large-scale flow. Open water currents will tend to avoid and flow around a region of extra drag associated with a turbine array, while the presence of turbines in confined channels will reduce the overall volume flux through the whole channel. The potential of a single turbine may be reasonably assessed using the natural flow, but the lower power will eventually offset the extra power from the addition of more turbines to an array due to a reduction in flow from the turbines already present. The maximum power P_{Max} (the theoretical resource) that can be achieved can be assessed only after taking large-scale backwater effects into account (Haas et al., 2011)

3.3 Hydrodynamic Model Data

To compute the parameters listed in Table 4, a year-long time series of depth-averaged velocity and water levels are required with fairly high spatial resolution across the US coastal waters. Hence, the tidal energy parameters were regenerated using data from

the national tidal energy resource assessment database, which used the Regional Ocean Modeling System (ROMS) model for hindcast simulations. The numerical model (ROMS) is a member of a general class of three-dimensional, free surface, terrain-following numerical models that solve three dimensional Reynolds-averaged Navier-Stokes equations (RANS) using the hydrostatic and Boussinesq assumptions. ROMS uses finite difference approximations on a horizontal curvilinear Arakawa C grid and vertically stretched terrain-following coordinates. Momentum and scalar advection and diffusive processes are solved using transport equations, and an equation of state computes the density field that accounts for temperature, salinity, and suspended-sediment concentrations. The modeling system provides a flexible framework that allows multiple choices for many of the model components such as several options for advection schemes (second order, third order, fourth-order, and positive definite), turbulence models, lateral boundary conditions, bottom- and surface-boundary layer submodels, air-sea fluxes, surface drifters, a nutrient-phytoplankton-zooplankton model, and a fully developed adjoint model for computing model inverses and data assimilation. The model also includes a wetting and drying boundary condition, which is essential for tidal flow simulations. The computational grids were set up, and the results were calibrated following the outlines of tidal stream modeling efforts for a regional study (Haas et al., 2011).

The national tidal energy resource database has 69 fields recorded for 1.65217 million grid points on the east coast and 1.5958 million grid points across the west coast of U.S. The 69 parameters include – geographical coordinates (latitude and longitude), the modeled depth, computed water level constituents and tidal depth-averaged current constituents, and one-month mean/maximum for tidal current speed and tidal stream power

density. The information regarding the tidal constituents includes the constituent name (Q1, O1, P1, K1, N2, M2, S2, K2, M4, M6), amplitude and phase (with respect to Greenwich) for water level; a major and a minor axis amplitude, phase, and inclination angle for the tidal current. For the USA East Coast and the Gulf of Mexico, the ROMS tidal forcing file is generated by interpolating the ADCIRC tidal database at the open boundary nodes of the ROMS grid. The harmonic constituents used for the forcing include Q1, O1, K1, S2, M2, N2, K2, M4, and M6. For the USA West Coast and Alaska domains, TPXO data, with the constituents Q1, O1, K1, S2, M2, N2, and M4, are used (Defne et al. 2012).

3.4 Generation of time series

Reconstruction of the yearly time-series of water level (e.g. Figure 8) and depth-averaged current velocity (e.g. Figure 9) for each grid point is done using the MATLAB toolbox, t_tide_v1.3 beta (Pawlowicz, 2002), based on all the tidal constituents in the national tidal assessment database.

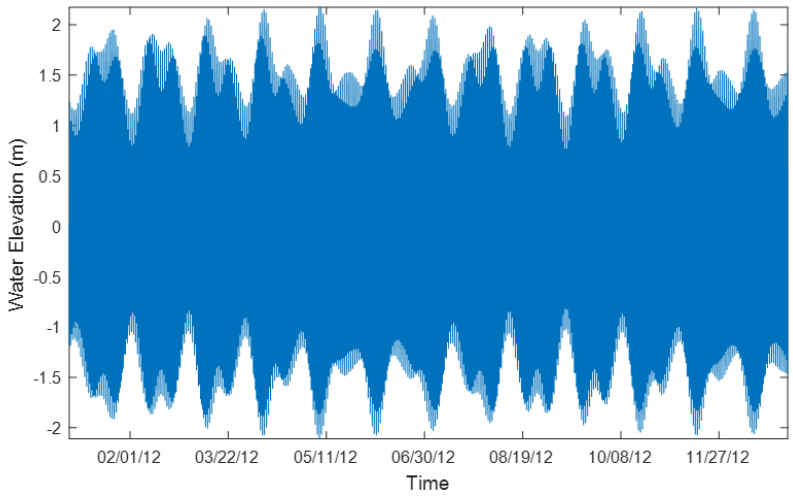

Figure 8 Tidal water elevation time series regenerated from the National Tidal Assessment Database at Portland, ME (43.655 N, -70.2467 W).

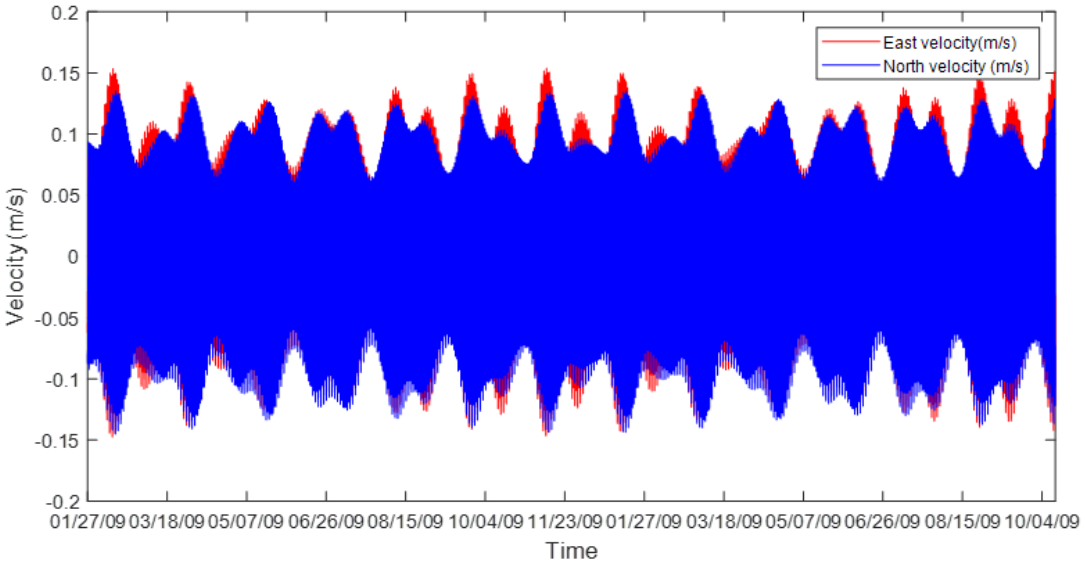

Figure 9 Tidal depth-averaged current velocity time-series regenerated from the National Tidal Assessment Database at Portland, ME (43.655 N, -70.2467 W).

To verify the method for computing the annual time series, yearly time series of water elevations generated were validated for ten sites (Figure 10) on the east coast against the in-situ tidal gauge data available at NOAA's website (NOAA, 2019). Figure 11 shows an example of water level comparisons between regenerated time-series and NOAA's data for one of the ten sites checked. Based on the recommendations for skill assessment methods for tidal resource modeling by NRC, the root mean square error (RMSE) between the observed and model time series is computed to evaluate the model skill (NRC, 2013). The following equation is used for the calculation of the RMSE values for all the sites across the U.S.:

$$RMSE = \sqrt{\frac{\sum_{i=1}^{N}(M_i - O_i)^2}{N}} \quad (3)$$

where M_i is the regenerated time-series data, O_i is the corresponding observed value from NOAA, and N is the total number of values in the time-series. As seen in Table 5, the method used to reconstruct the time series is credible, as the RMSE values are minimal for all the places with significant RMS water elevation values. The tidal gauge data for shallow water elevation, indicated by low RMS values in Table 5, are implicit with higher error, hence relatively higher values of RMSE for those stations. But the low RMSE values for Portland, Boston, which have relatively higher RMS values verify the correctness of the method to reconstruct the time series, as there is an excellent match between the field measured data and the hydrodynamic model data.

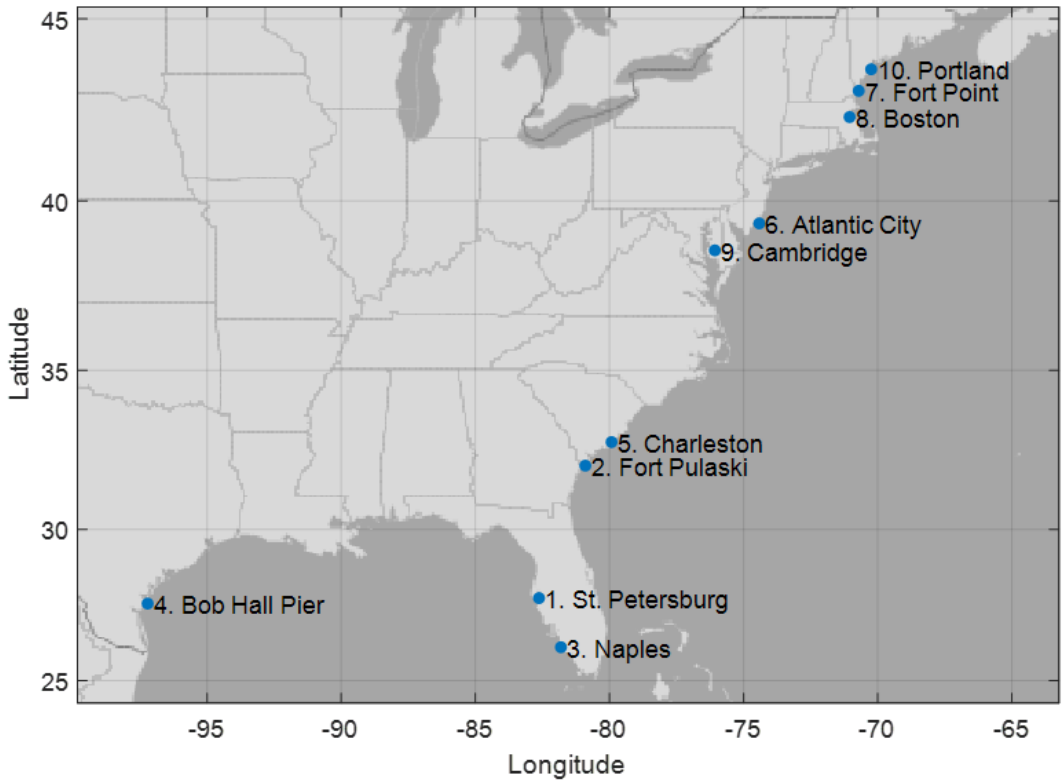

Figure 10 Ten locations on the U.S. east coast used for validating the annual time-series generation methodology.

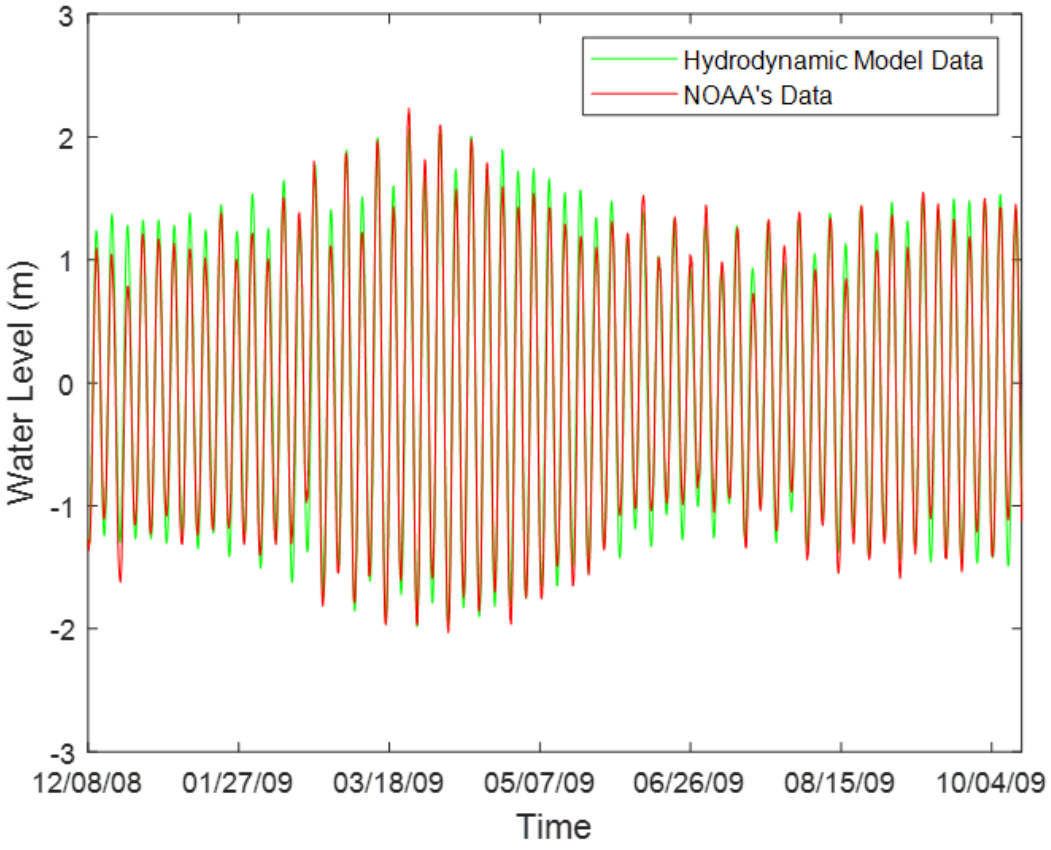

Figure 11 The water elevation time-series from hydrodynamic model data and the observed NOAA's data at one of the ten selected sites, Portland, ME (43.655 N, -70.2467 W).

Table 5 Root mean square errors (RMSE) for the hydrodynamic model data, compared to NOAA's data for ten sites on the U.S. east coast for verification of model data regeneration method.

Longitude	Latitude	Location Name	RMSE (m)	RMS (m)
-82.627	27.76	St. Petersburg, Tampa Bay, FL	0.248	0.292
-80.9017	32.0367	Fort Pulaski, GA	0.328	0.779
-81.8083	26.1317	Naples, Gulf of Mexico, FL	0.212	0.321
-97.2167	27.58	Bob Hall Pier, Corpus Christi, TX	0.162	0.246
-79.9233	32.78	Charleston, Cooper River Entrance, SC	0.252	0.614
-74.4183	39.3567	Atlantic City, NJ	0.196	0.473
-70.71	43.0717	Fort Point, NH	0.196	0.952
-71.05	42.3533	Boston, MA	0.213	1.006
-76.0717	38.575	Cambridge, MD	0.202	0.252
-70.2467	43.655	Portland, ME	0.209	1.001

3.5 Year selection for further data analysis

The variation of water level computed in the previous section is due to the rotation of the earth and the gravitational pull of the sun and moon. This phenomenon of changing the water level is very sensitive to the relative positions of the moon, sun, and earth. The orbit of the moon undergoes two essential types of precessional motions – Apsidal and nodal. The Apsidal precession is the rotation of the major axis of the moon's elliptical orbit. One complete Apsidal precession cycle takes place in 8.85 years. The second type of lunar precession is of the plane of the moon's orbit. Nodal precession is the precession of the orbital plane of the moon around the rotational axis of the earth. Its period is about 18.6 years.

Nodal precession is the most considerable influence in diurnal regions, with tide ranges greater than 4m. The nodal modulation can range from 0.5-0.8 m for the areas dominated by diurnal tides (Haigh et al., 2011).

To identify the best year for analysis, yearly mean current speed were compared for nine years, 2009-2017. The mean annual tidal current variation can be observed for nine years in Figure 12(a) and the deviation of mean tidal yearly current from the collective mean of the mean annual tidal current values of nine years in Figure 12 (b). It can be inferred from the figures that the mean annual currents are increasing from 2007 to 2015. Based on the variation in the tidal currents due to the nodal cycle, 2015 was selected as the year for further analysis, because we wanted to review the range of flows based on the maximum occurring conditions.

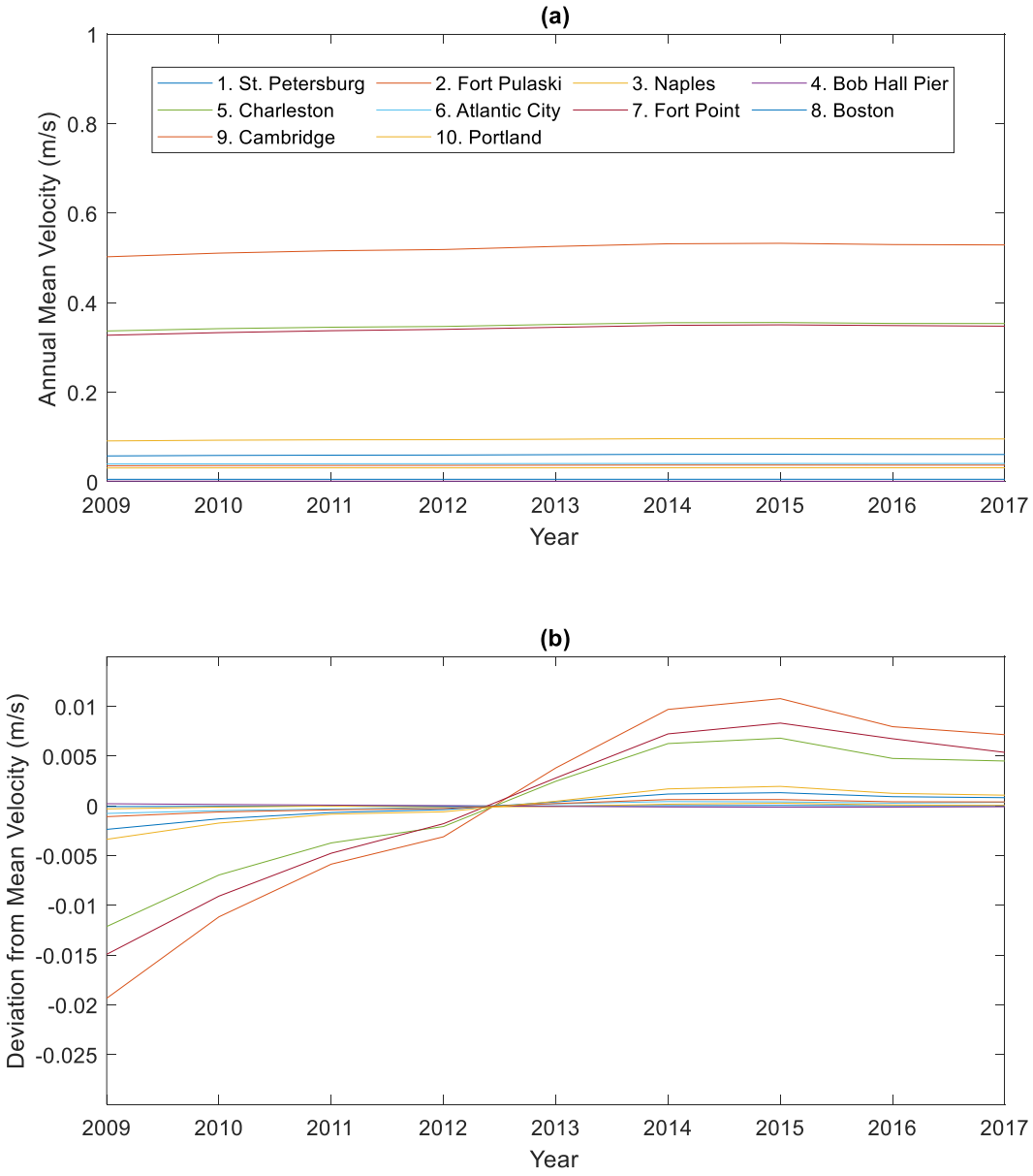

Figure 12 (a) Annual mean depth-averaged velocity magnitude for ten sites listed in table 5, (b) deviation of annual mean velocity from the mean of mean yearly velocities of all the nine years for ten different locations listed in Table 5.

3.6 Tidal Data Subsetting

To identify the relevant portions of the data set to facilitate the analysis for finding suitable classification parameters, the annual mean velocity is computed for all the grid points in the national tidal assessment database. Figure 13(a) shows an occurrence histogram of mean velocities for all the grid points across the U.S. As 96% of the mean velocity values computed at 3,118,538 grid points are less than 0.5 m/s, which does not amount to substantial potential for tidal energy harnessing, the tidal data was filtered for much of the further analysis. The velocities computed at all the grid points in the national tidal assessment database was screened for all the velocities higher than 0.5 m/s and for the sites with a depth greater than 5 m, to reduce the dataset to 129,444 grid points. Figure 13(b) shows an occurrence histogram of mean velocities for all the filtered grid points across the U.S.

To further facilitate a convenient reduction of data, a hundred and fifty-one hotspot locations were identified from the study performed by Defne et al., 2012, and the list was augmented by the nineteen additional hotspots recognized by Kilcher et al., 2016. Hence, the data was further filtered down for a more detailed analysis of tidal parameters, to 21,871 grid points in the vicinity (+/- 0.3 degree) of the 170 identified hotspots. The filtered dataset for 170 hotspots is shown in Figure 13 (c). For convenience, the term hotspot dataset is used to refer to this dataset in the rest of the study.

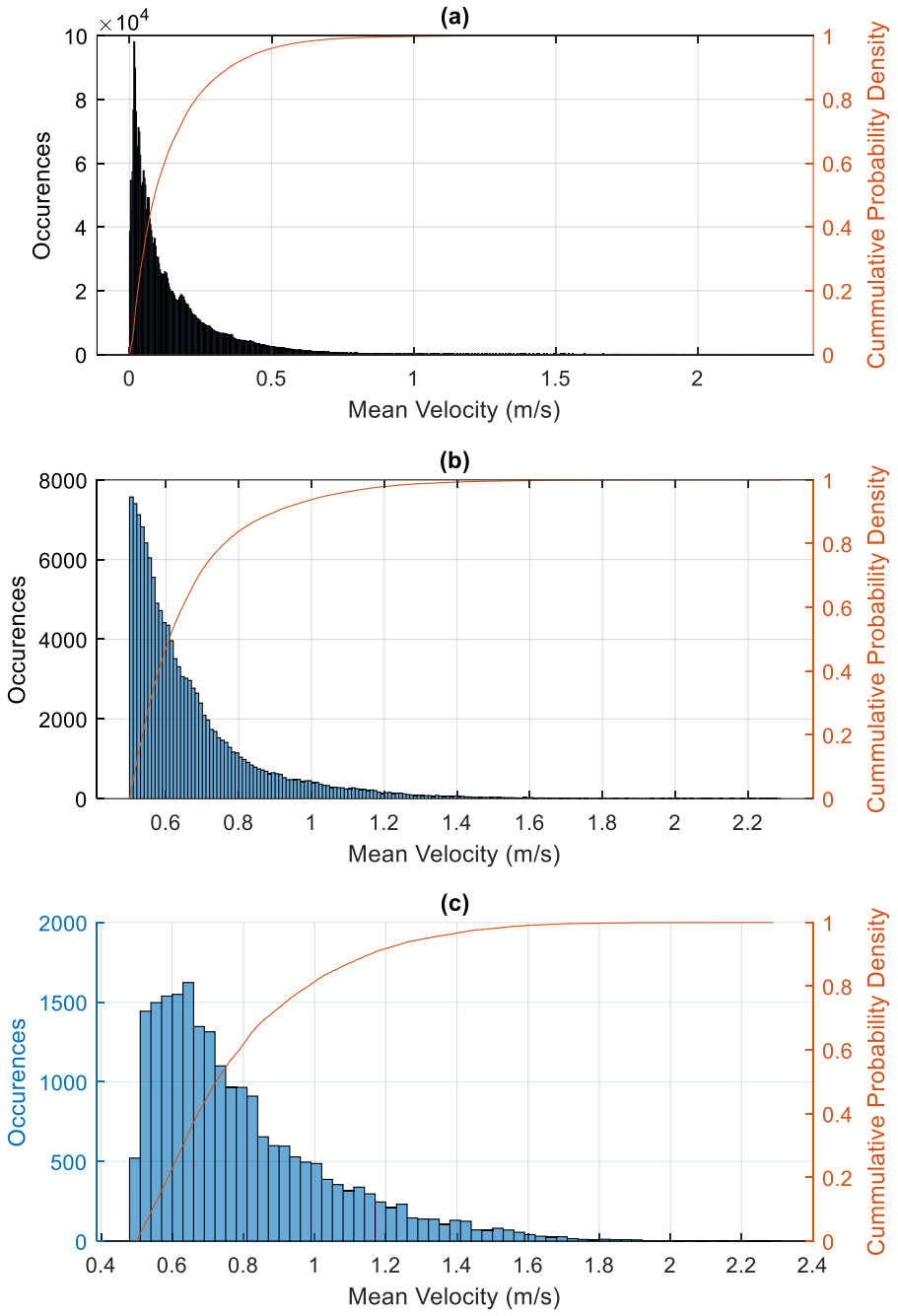

Figure 13 Mean velocity occurrence histogram, and cumulative probability density function of mean velocity, (a) for all the grid points across the US coast, (b) for locations with a mean velocity higher than 0.5 m/s and depth >5m, (c) for 170 hotspots, from the national tidal assessment database and Kilcher et al., 2016.

3.7 Primary Parameter

For tidal resource classification, like wind energy, power density is the primary parameter for the classification system. To facilitate preliminary project planning and development of tidal devices, it is convenient to establish a relationship between the characteristic design parameters and the primary classification parameter such that the design parameters could be gleamed from the fundamental parameter without extensive data processing. In that endeavor, the following section discusses the relationship between the mean velocity and the primary classification parameter. In addition, various design parameters have been studied to propound their relationships with the mean velocity.

For tidal device classification, the mean current speed characterizes the normal tidal condition, whereas the peak current velocity, e.g., the perigean spring tidal current occurring three to four times a year, portrays the extreme tidal condition and is a likely candidate for the reference, current speed in the device classification system (Neary et al., 2019). Hence, the maximum current velocity and other device classification parameters have been correlated to mean velocity to study their relationship.

Further, in this section, to identify and group the sites with various ranges of availability and scale of tidal energy for harnessing, the primary classification parameter has been sorted into four classes based on various schemes, and the final categorization scheme to delineate the categories is established.

3.7.1 Relationship between different parameters

In this study, it was determined that the annual mean current is highly correlated with 1% exceedance velocity and annual maximum tidal current speeds, with the Pearson correlation coefficient of 0.93 and 0.896, respectively (see Figures 14 and 15). The regression line linearly defines their relationships, and the figures show their relationship equations. Hence, once we know the mean velocity at a location, we can also surmise the magnitude of the one percent exceedance and maximum velocity at that location. These relationships would be beneficial in tidal device development and classifications, which is a prospective augmentation of the work performed in this study.

Further, the relationship between the mean power and the mean velocity is found by computing the power density from the mean velocity and comparing it to mean power density, as shown in Figure 16 below. A best-fit line is found to give a relationship Pm ~ 1.75 times the power calculated from mean velocity. This relationship is used to find the mean velocities corresponding to the mean power density chosen to define the resource classes, which is discussed in the next section.

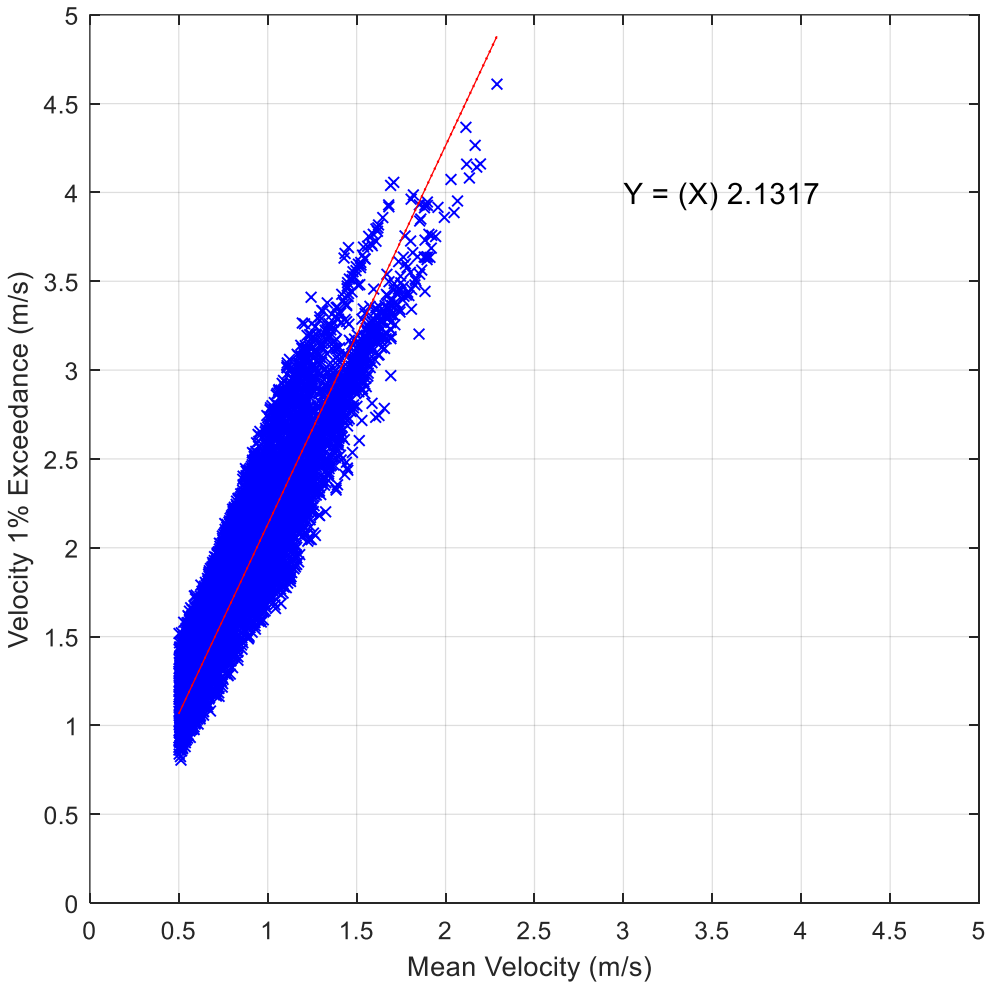

Figure 14 Scatter plot between Mean Velocity (V>0.5m/s) and 1% Exceedance velocity. The equation of best fit line, passing through origin is displayed on the plot. Coefficient of correlation for these two parameters, R=0.9315.

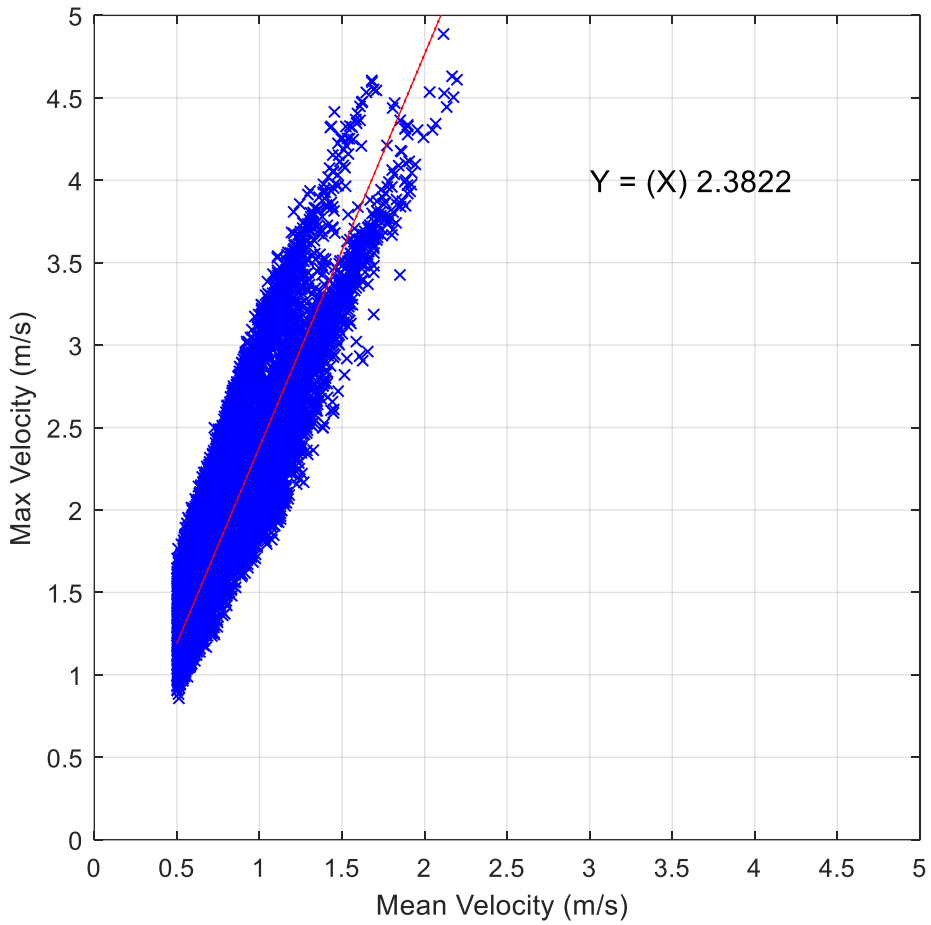

Figure 15 Scatter plot between annual mean velocity (V>0.5m/s) and annual maximum velocity. The equation of best fit line, passing through origin is displayed on the plot. Coefficient of correlation for these two parameters, R=0.8966.

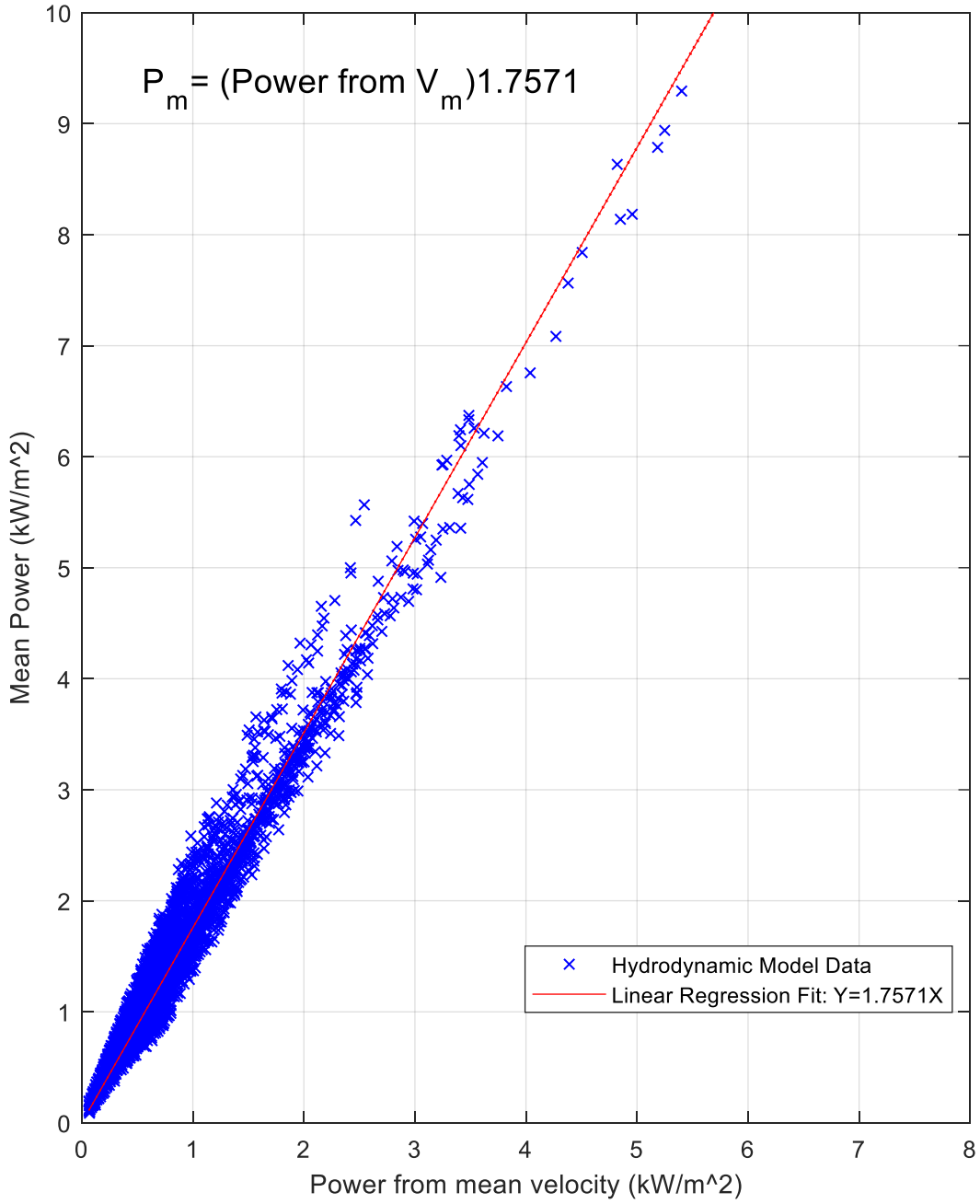

Figure 16 Relation of the mean power density (P_m) to the annual mean velocity (V_m) and the equation defining their relationship.

3.7.2 Delineating primary parameter classes

There were various delineation methods considered for categorizing the primary parameter for tidal resource classification. The power density data for all the 170 hotspot locations (hotspot dataset), were divided into four classes based on the following methods.

3.7.2.1 Type 1: Using the mean of velocity

To categorize the mean velocity data into four classes, three class dividing values (C_{11}, C_{12}, C_{13}) based on the mean and plus/minus one standard deviation are defined in the equations (4)-(6) below.

$$C_{11} = \sum_{i=1}^{N} \frac{v_i}{N} \tag{4}$$

$$C_{12} = \sum_{i=1}^{N} \frac{v_i}{N} + \sqrt{\sum_{\mathrm{i=1}}^{\mathrm{N}} \frac{(C_{11} - v_i)^2}{\mathrm{N}}} \tag{5}$$

$$C_{13} = \sum_{i=1}^{N} \frac{v_i}{N} - \sqrt{\sum_{i=1}^{N} \frac{(C_{11} - v_i)^2}{N}} \tag{6}$$

where N is the number of points in the hotspot dataset, v_i is the annual mean velocity at a grid point in the hotspot database. This classification scheme is shown on the probability density function of mean velocity where the magenta color lines in Figure 17 represent the classes. Classes are divided at 0.55 m/s, 0.8 m/s, 1.05 m/s, which distributes the hotspot

locations across the U.S. into classes IV to I containing 10%, 51%, 23%, 16% of the points, respectively.

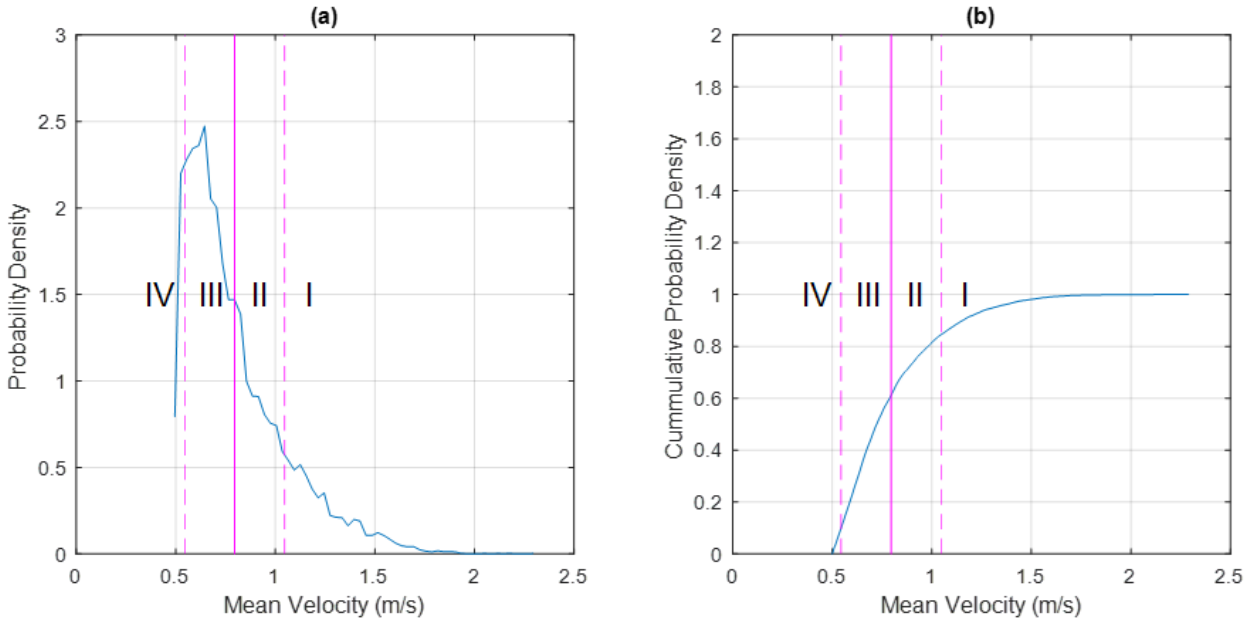

Figure 17 (a) Probability density function, (b) Cumulative density function of mean velocities. The type 1 classification scheme divides the hotspot locations around the U.S. in four classes. Here, solid line represents the mean of mean velocities and the dashed lines are mean of mean velocities +/- one standard deviation of mean velocity, which collectively divides the data into four classes.

3.7.2.2 Type 2: Using the mean of power density

To categorize the power density data into four classes, three class dividing values (C_{21}, C_{22} and, C_{23}) of power densities were computed based on the mean of annual mean power density at all the grid points in the hotspot dataset (Equation 7), mean of annual mean power densities + standard deviation of mean power densities (Equation 8), and mean of annual mean power densities - standard deviation of mean power densities (Equation 9).

$$C_{21} = \sum_{i=1}^{N} \frac{P_i}{N} \tag{7}$$

$$C_{22} = \sum_{i=1}^{N} \frac{P_i}{N} + \sqrt{\sum_{i=1}^{N} \frac{(C_{21} - P_i)^2}{N}} \tag{8}$$

$$C_{23} = \sum_{i=1}^{N} \frac{P_i}{N} - \sqrt{\sum_{i=1}^{N} \frac{(C_{21} - P_i)^2}{N}} \tag{9}$$

where P_i is the annual mean power density at a grid point in the hotspot dataset and, N is the total number of grid points in the hotspot dataset. Blue lines in Figure 18 represent this classification scheme. The 4 classes are divided at: -86.19 W/m^2, 627.94W/m^2, 1342.1 W/m^2. The distribution of the hotspot sites into classes IV to I is 0%, 70%, 19%, 11%

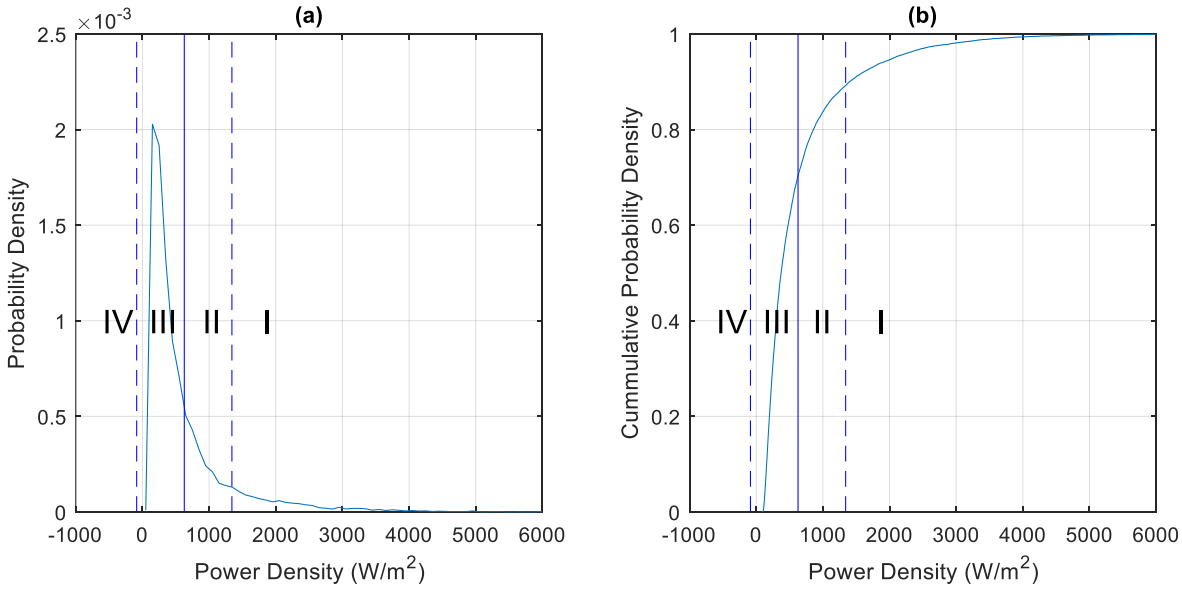

Figure 18 The type 2 classification scheme, divides the hotspots locations around the U.S. in four classes. Here, solid line represents $\boldsymbol{C_{21}}$ and the dashed lines are $\boldsymbol{C_{22}}$ and $\boldsymbol{C_{23}}$.

respectively. This scheme was disregarded right away as the lowest class division value is negative and hence a meaningless value for power density.

3.7.2.3 Type 3: Using the mean of power density and standard deviation of mean velocity

In the type three categorization scheme, the primary classification parameter is also divided into four classes. The central dividing line is based on the annual mean power density, represented by the black vertical lines in Figure 19. The velocity corresponding to the mean power density (v) is calculated using equations (10).

$$v = (2P_M / \rho)^{1/3} \tag{10}$$

where P_M is the mean power density, ρ is the density of seawater. The other two class dividing lines are calculated using the standard deviation of the annual velocity (v_{std}) by using equations (11).

$$P = 0.5\rho(v \pm v_{std})^3 \tag{11}$$

Hence, the class dividing values are evaluated, and classes are divided at 282 W/m^2, 628 W/m^{2,} and 1180.5 W/m^2. The distribution of the sites into four classes is 36%, 34 %, 17%, 13%, in decreasing order of classes.

3.7.2.4 Type 4: Using the log of power density

To categorize the power density data into four classes in type 4 scheme, three class dividing values for log of power densities were computed based on the mean of log of

power densities, mean of log of power densities + standard deviation of the log of power densities and mean of log of power densities - standard deviation of the log of power densities. This classification scheme is represented by cyan color in Figure 20. Classes are: 184.88 W/m^2, 424.15 W/m^2, 972.92 W/m^2. The distribution of the sites into 4 classes is 17%, 38 %, 28%, 17% respectively.

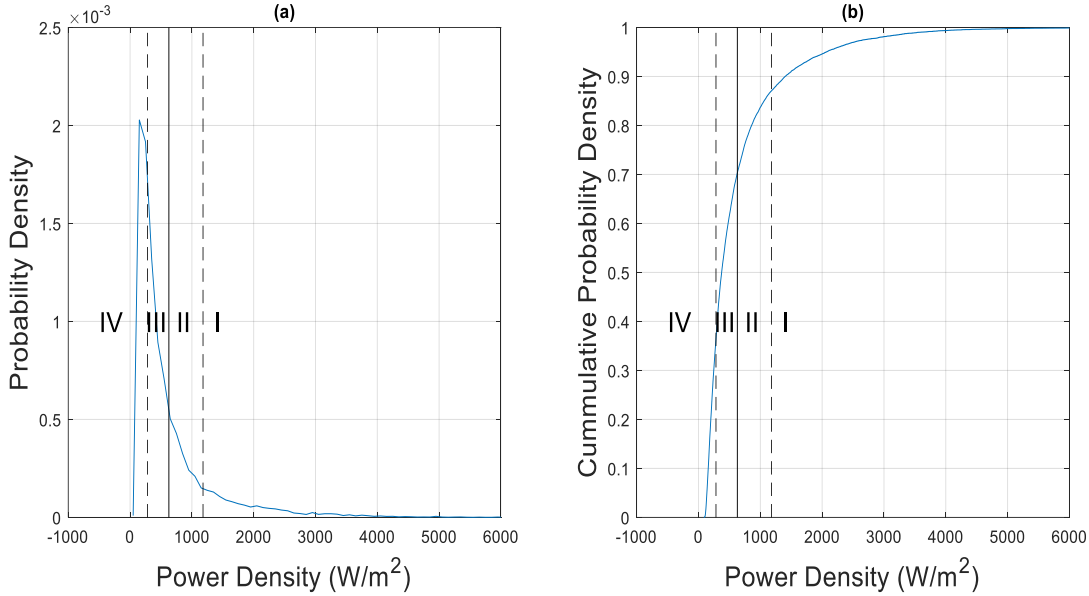

Figure 19 The type 3 classification scheme divides the hotspots locations around the U.S. into four classes.

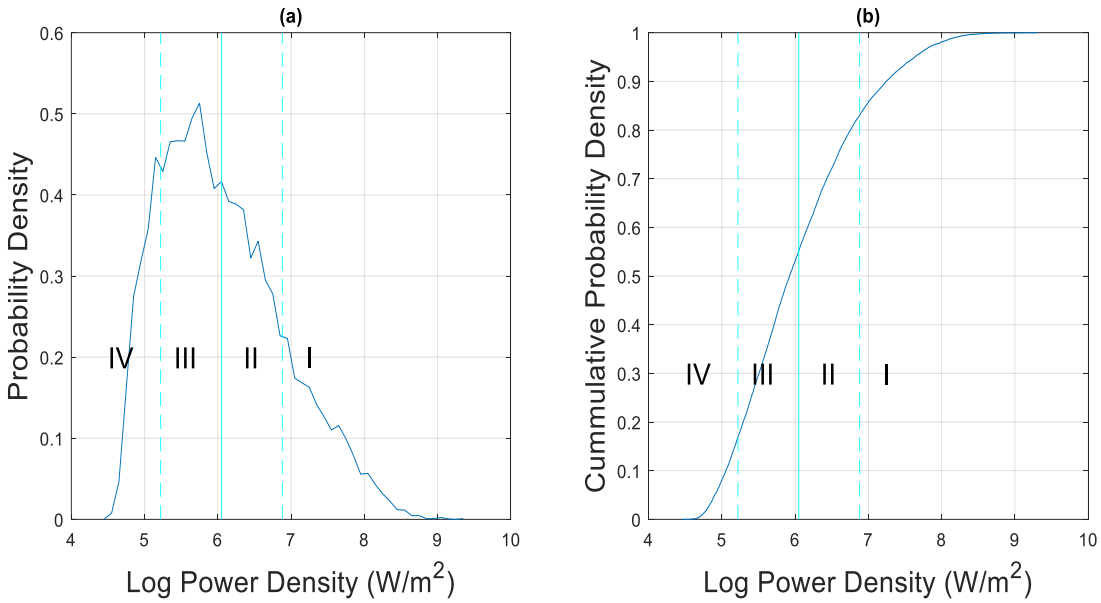

Figure 20 The type 4 classification scheme divides the hotspots locations around the U.S. into four classes.

Considering all the classification types in the section above, they were compared together in Figure 21. Type 2 classification scheme was disregarded, as class four was non-positive, which is technically incorrect to be considered as a power class. Type 1, 2, and 4 give a better classification system than type 2, but these schemes divide the higher power sites into a single, very large range (Table 6). To utilize the classification system in device development, it is preferable to divide the high-power density, viable tidal energy project sites into a smaller range of values. Hence, after considering the above mentioned four types of classification approaches and preliminary discussions with the developers, the four power classes were delineated, as shown in Table 7 below. The final classification system was fundamentally based on type 1, but the higher range of power density was further bifurcated at mean velocity, 1.3 m/s, and the lowest division class was disbanded.

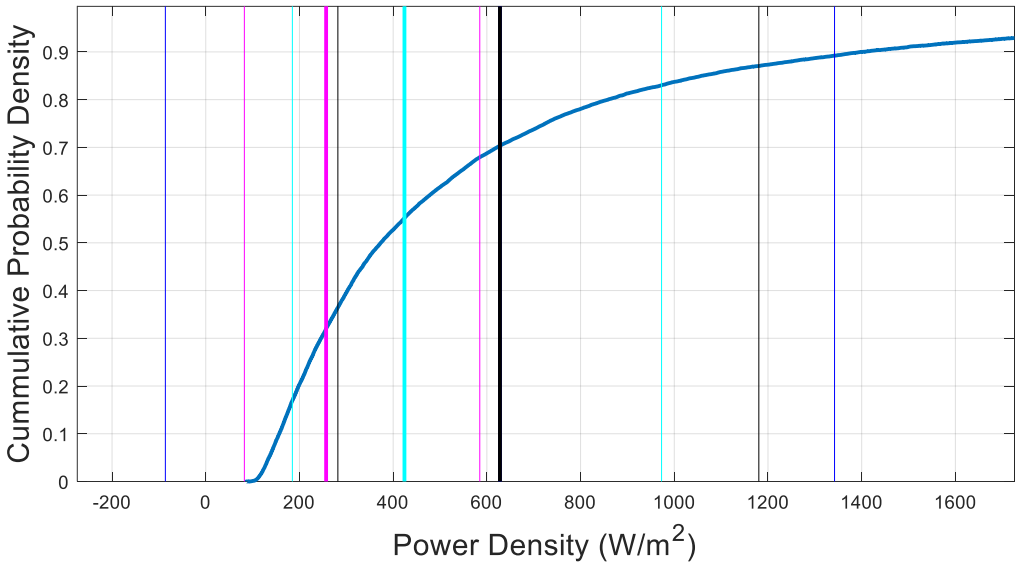

Figure 21 The four types of classification schemes for primary classification parameter – Type 1 is in Magenta, Type 2 is in Blue, Type 3 is in Black, and Type 4 is in Cyan.

Table 6 Four types of primary parameter classification schemes and their respective classes. Here, $\boldsymbol{V_m}$ is mean velocity, and $\boldsymbol{P_d}$ is power density.

	Type 1 (kW/m^2)	Type 2 (kW/m^2)	Type 3 (kW/m^2)	Type 4 (kW/m^2)
Class I	$V_m \geq 1.05$	$P_d \geq 1.3$	$P_d \geq 1.18$	$P_d \geq 0.97$
Class II	$0.8 \leq V_m < 1.05$	$0.6 \leq P_d < 1.3$	$0.63 \leq P_d < 1.18$	$0.42 \leq P_d < 0.97$
Class III	$0.55 \leq V_m < 0.8$	$0.086 \leq P_d < 0.6$	$0.28 \leq P_d < 0.63$	$0.18 \leq P_d < 0.42$
Class IV	$V_m < 0.55$	$P_d < 0.086$	$P_d < 0.28$	$P_d < 0.18$

In Table 7, based on the power classes, the corresponding mean velocities were also computed using the method explained in section 3.7.1. For example: for class I of the final classification, the mean power is 2 kWh/m^2. Using the relationship in Figure 16, the power density calculated from mean velocity corresponding to mean power is found by dividing the mean power of class by 1.75. And the mean velocity for that class is computed from

the mean velocity power, by plugging the power into $v = (2P_M / \rho)^{1/3}$. Hence, we get the velocity for class I equal to 1.3 m/s.

Finally, the four classes defined by the annual mean velocity are shown in Figure 22. The final classification scheme selected has 62% of the hotspot sites in class IV, 23%, 10%, and 5% in class III, II, and I, respectively.

Table 7 Primary parameter classification scheme for Tidal Energy Resource Classification

Power Class	***I***	***II***	***III***	***IV***
Power Density (kWh/m^2)	$P \geq 2$	$1 \leq P < 2$	$0.5 \leq P < 1$	$P < 0.5$
Mean Velocity (m/s)	$V_m \geq 1.3$	$1.05 \leq V_m < 1.3$	$0.8 \leq V_m < 1.05$	$V_m < 0.8$

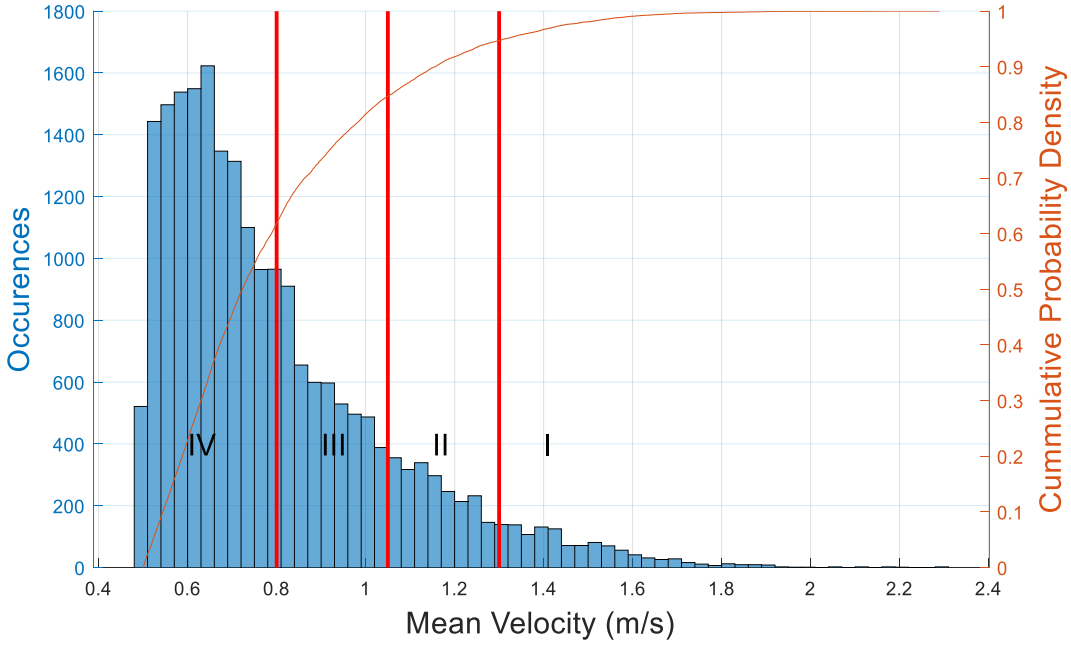

Figure 22 Primary parameter classification scheme based on mean velocity. Histogram shows the frequency of occurrences of mean velocity across the U.S. coast and the cumulative density function of mean velocity.

3.8 Secondary Parameter

The technical resource is defined as the amount of energy that can be extracted using a particular technology. The portion of the theoretical power available at a site that can be captured is contingent on many physical and technical constraints. The DoE identifies these constraints as physical and technological filters. Some of these filters being resource-specific apply to all the MHK resources. Hence, to have a more realistic framework of available energy, we need another parameter to filter the resource based on a general physical constraint (NRC, 2013).

The power density and mean velocity provide an excellent fundamental classification for tidal stream resource availability, but it does not appraise the scale and magnitude of the total power available at the site. It can be further noted from Figure 23, which shows the maximum power for the US hotspots as a function of mean velocity, though the mean velocity at a location qualifies a place for project consideration; it is not a complete assessment of extractable power. Hence, various parameters were inspected for their suitability for the secondary resource classification. The variables analyzed in this study are depth, width, surface area, and cross-sectional area of the stream. The essential idea behind selecting a secondary parameter is its capability to reflect the total amount of energy available at a location. In that context, the cross-sectional area reflects the total flow flux, so it provides guidance on the potential of overall energy extractable at a site. The surface area is also considered as a secondary parameter, although it is not related to the volume flux, it is the measure of the area available for the tidal array, hence the scale of the project. Additionally, physical stream parameters such as depth and width were also considered as they are the constraining factor for the installation of tidal devices and arrays, respectively.

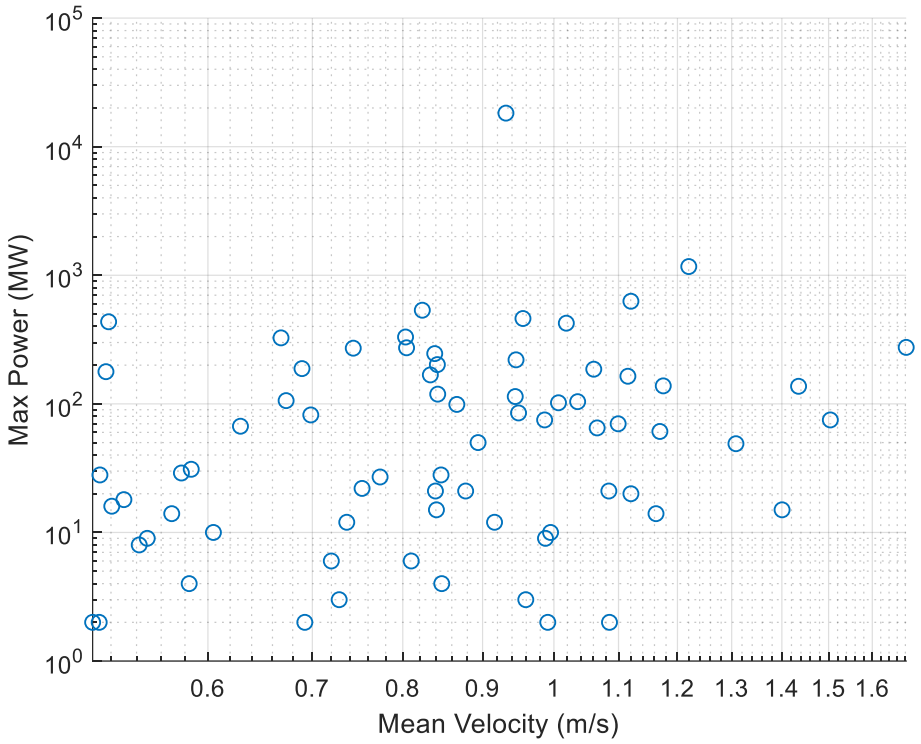

Figure 23 Scatter plot of mean velocity vs. max power for all the hotspot locations around the US coast from the national tidal resource assessment report. R=0.043.

The data for the physical parameters mentioned above were collected from the extensive national tidal assessment done by Haas et al., 2011. The occurrence histograms for hotspot widths, cross-sectional areas, and surface areas are shown in Figures 24-26.

It can be observed from Figure 24, 28% of the hotspot sites have a width of less than a kilometer, and 92% of the sites fall below 10 km. In Figure 25, 93% of the sites have a cross-section area less than a kilometer squared and rest 7% of the sites have a cross-section varying from 1 to 8 km^2. Similarly, for surface area (Figure 26), 22% of sites have a surface area less than a km^2, 55% of the locations fall below 10 km^2, and 81% are below 100 km^2. The only outlier in the data is the Cook Inlet, with 93,780 m width and surface area of 18,239 km^2.

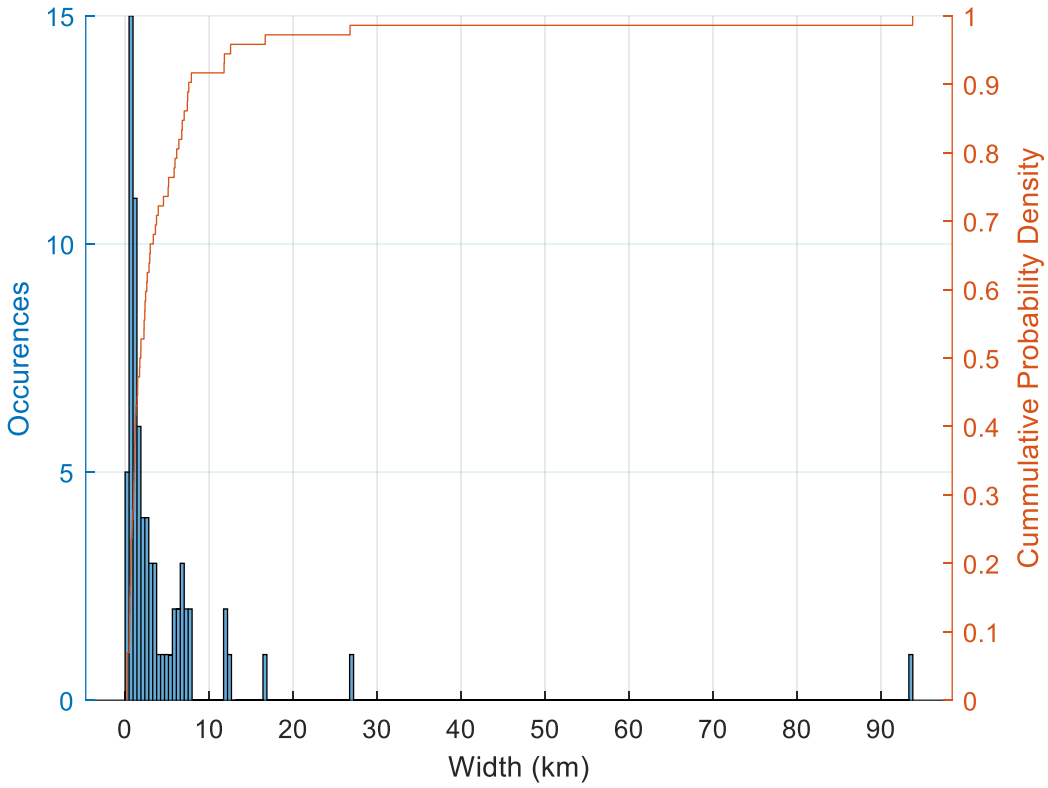

Figure 24 Width data of all the hotspot locations around the US coast from the national tidal resource assessment report (Haas et al., 2011).

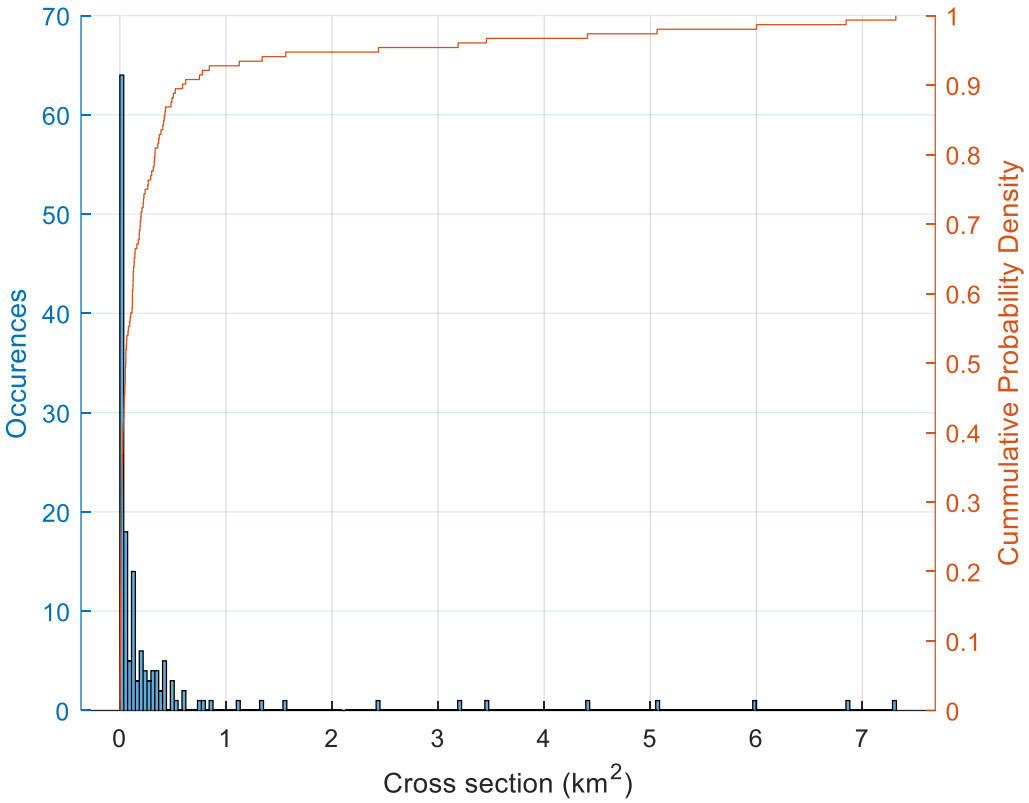

Figure 25 Cross-section area data of all the hotspot locations around the US coast from the national tidal resource assessment report (Haas et al., 2011).

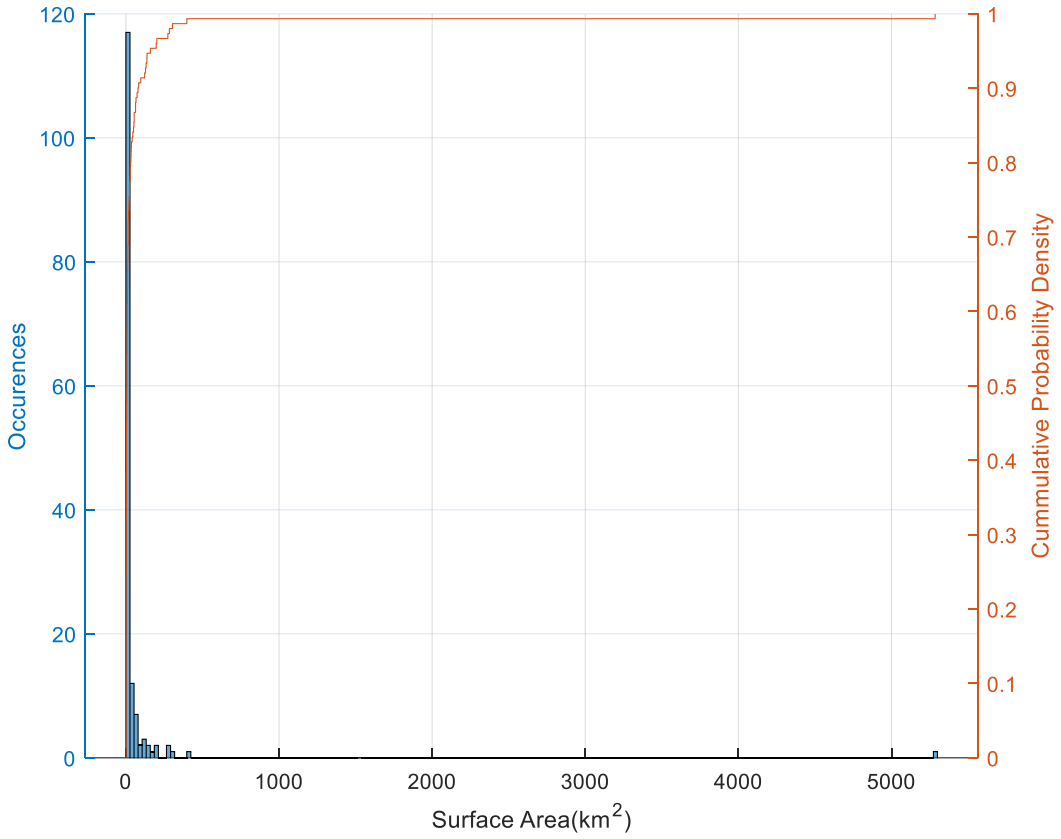

Figure 26 Surface Area data of all the hotspot locations around the US coast from the national tidal resource assessment report (Haas et al., 2011).

Also, as we established relationships between several parameters with the primary classification parameter in the previous section, similar efforts were made to gleam any relationship between the cross-sectional parameter and mean velocity. Hence, several scatter plots were created (Figure 27-30), but no significant correlation was observed to infer a robust relationship. Mean velocity is related to width (Figure 24), depth (Figure 25), cross-section (Figure 26) and surface area (Figure 27) by a Pearson correlation coefficient of 0.2, 0.06, 0.08, -0.1 respectively. It can also be observed from the figures that there are several locations with diverse physical parameter values for a particular annual mean velocity. Moreover, the mean velocity at a location is a function of several factors, such as

bathymetry, the rate of change of channel shape, etc., so it's not prudent to assume any explicit relationship of the physical parameters with the annual mean velocity at a location.

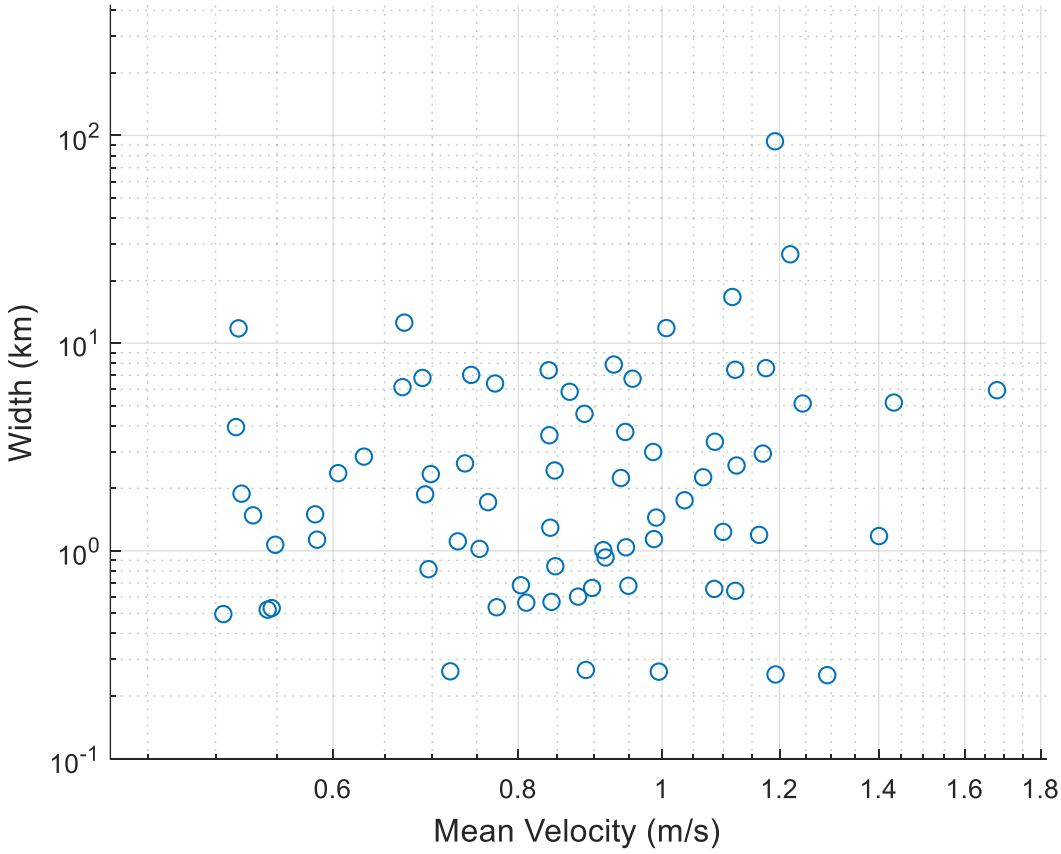

Figure 27 Scatter plot of mean velocity vs. width for all the hotspot locations around the US coast from the national tidal resource assessment report. R=0.2.

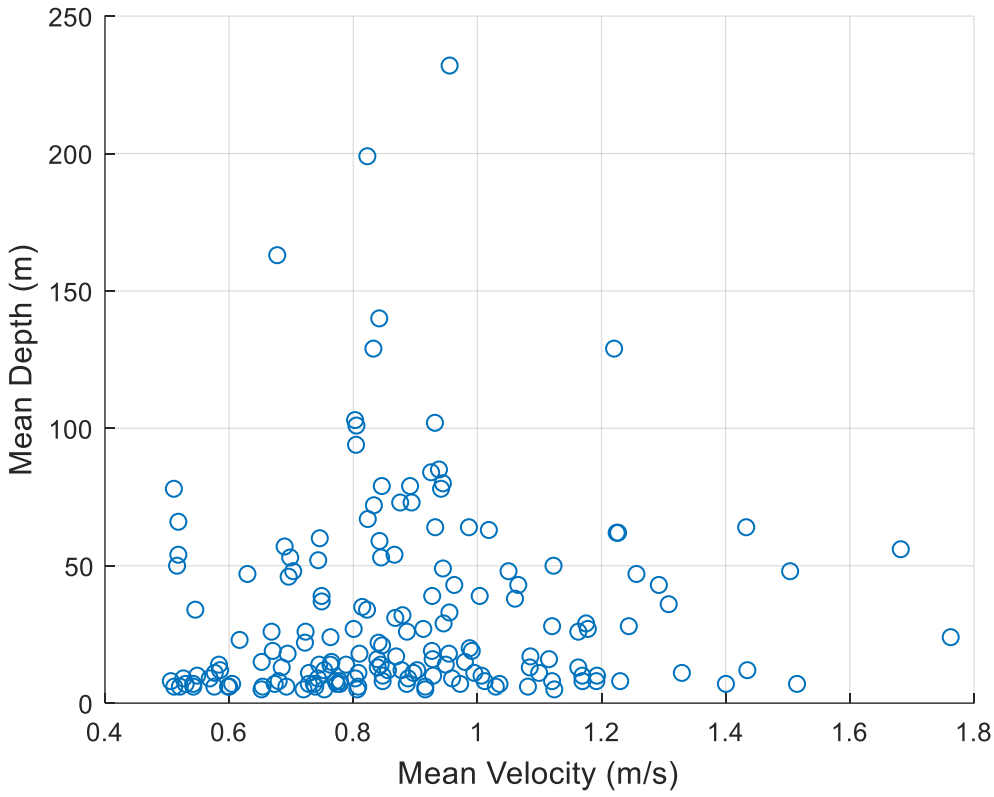

Figure 28 Scatter plot of mean velocity vs. depth for all the hotspot locations around the US coast from the national tidal resource assessment database. R=0.061

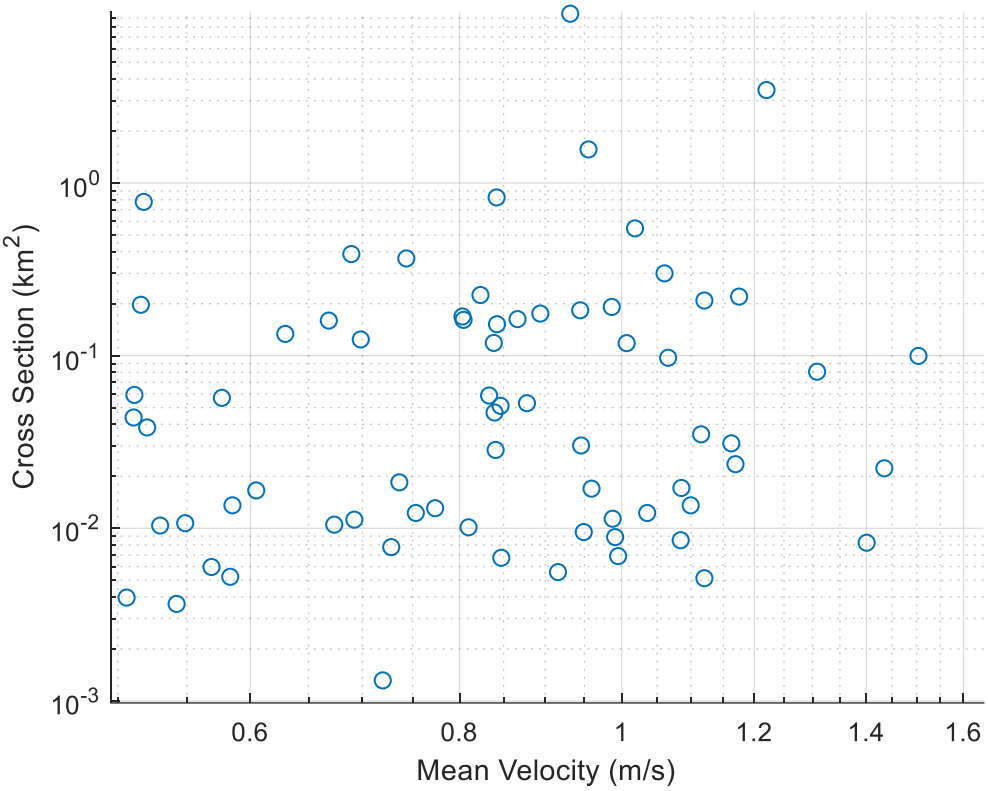

Figure 29 Scatter plot of mean velocity vs. cross-section area for all the hotspot locations around the US coast from the national tidal resource assessment report. R=0.08

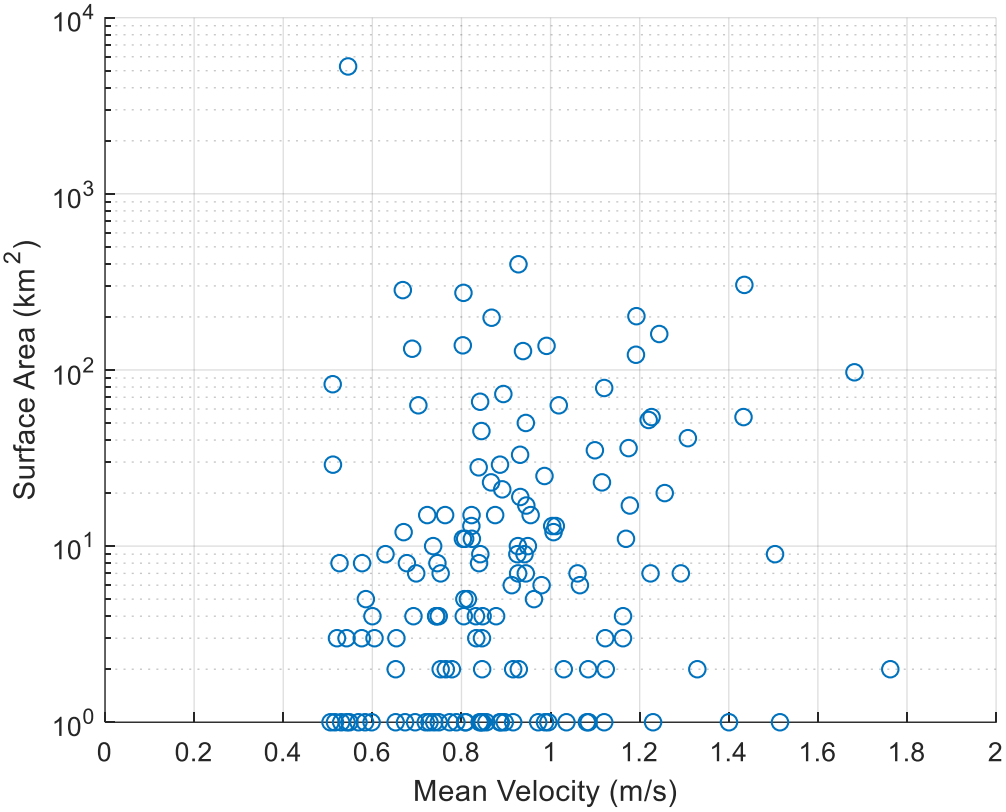

Figure 30 Scatter plot of mean velocity vs. surface area for all the hotspot locations around the US coast from the national tidal resource assessment report. R= - 0.1.

As all the parameters considered here reflect the physical scale of the tidal stream, it was speculated that these parameters would have some correlation with the maximum theoretical power available. So, the parameters were checked for their relationship with the max power, and if we find a sufficient correlation of a parameter with maximum power available, it would conveniently be used as the proxy of the available power and hence would be a measure of extractable energy.

For estimating the maximum theoretical power availability, it is vital to consider the far-field backwater effect. These backwater effects cause the reduction of the potential of available power due to the presence of extraction devices. Especially for the tidal, ocean,

and marine thermal currents, it is essential to consider far-field effects for the correct estimation of resources. Here, for considering the drag due to the placement of devices or device array, the reduced maximum theoretical power is estimated by the Garrett and Cummings method (Garrett and Cummins, 2005). Defne et al. already performed this analysis in 2012, for all the hotspot locations across the U.S; therefore, for finding a secondary parameter, the available data for hotspots was utilized for further statistical computations.

As the computation of maximum theoretical power is a tedious process, finding a suitable proxy parameter for that would ease the process of resource classification and site selection. Therefore, the potential candidate secondary parameters were studied for their correlation with a power density (Figure 31) and max theoretical power available (Figure 32-33). It can be observed, though the higher depths of channel exhibit lower power densities, no robust relationship could be established from Figure 31, which is also affirmed by a poor coefficient of correlation, R= - 0.16. Furthermore, the surface area was plotted against the max power to study any underlying semblance, but they lack any strong coherence (See figure 32). Still, it could be surmised that there is a weak trend of more significant surface area sites having more theoretical power available. The strong correlation coefficient of 0.95 between cross-section area and max theoretical power is a promising relation for the secondary parametrization (See figure 33). Hence, it could be concluded that the cross-sectional area is a fair proxy for maximum theoretical power available at a site, and it is easier to compute compared to maximum theoretical power. So, it was chosen as the secondary parameter for classification in this study.

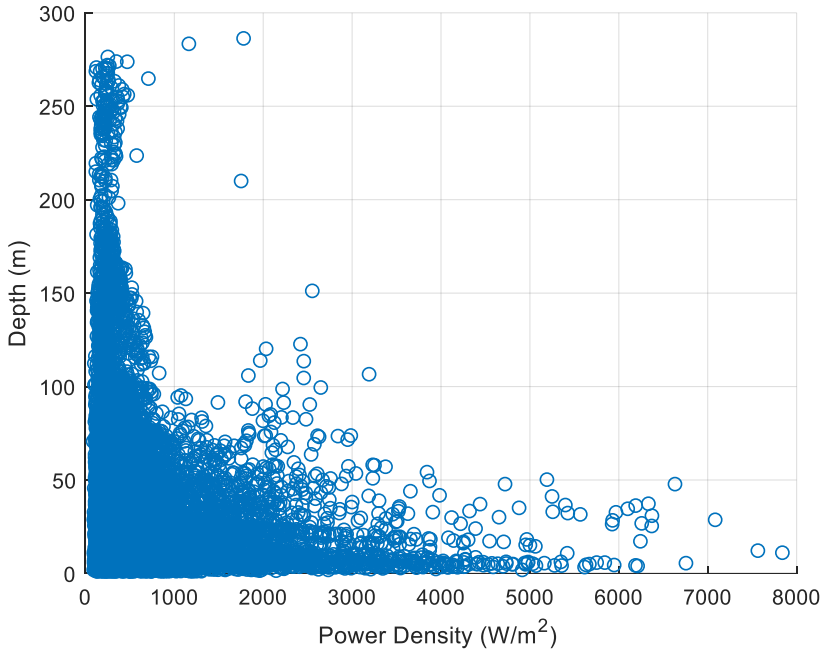

Figure 31 Scatter plot of power density vs. depth for all the grid points around 170 hotspot locations around the US coast (hotspot dataset). R= - 0.16.

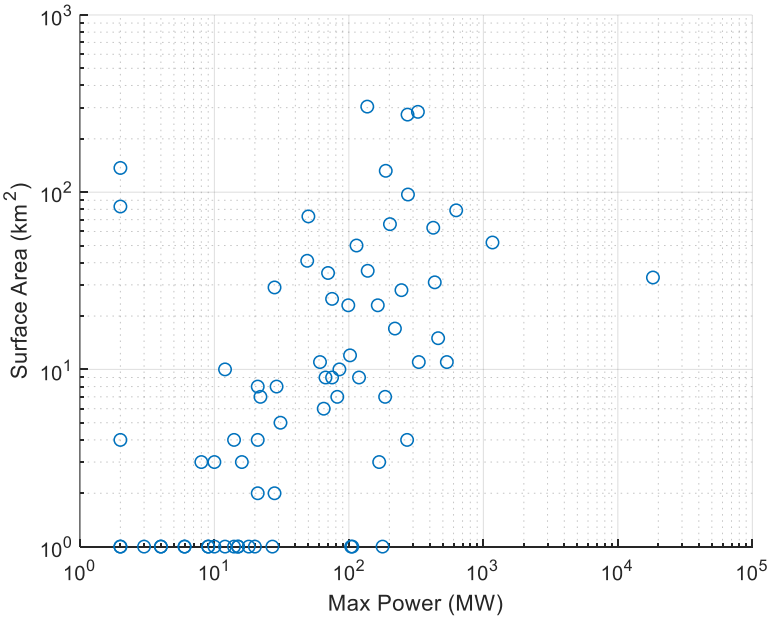

Figure 32 Scatter plot of maximum theoretical power vs. surface area for all the hotspot locations around the US coast from the national tidal resource assessment report (Haas et al., 2011). R=0.026.

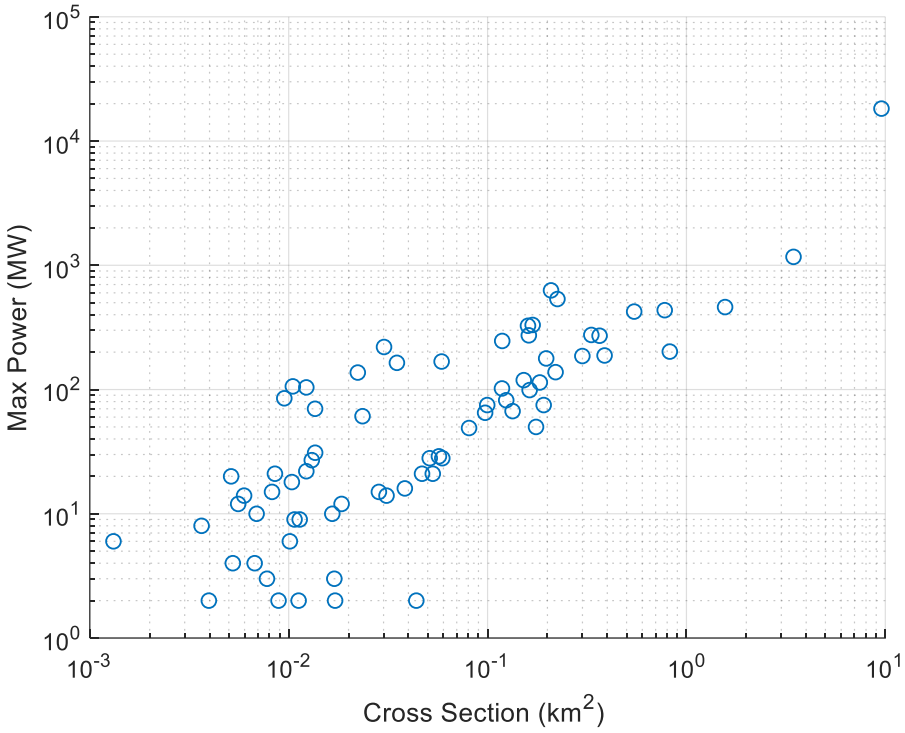

Figure 33 Scatter plot of maximum theoretical power available vs cross-sectional area for all the hotspot locations around the US coast from national tidal resource assessment report (Haas et al., 2011). R=0.95.

3.9 Resource classification classes

As the final secondary parameter, the cross-sectional area was separated into three classes (Figure 34). The dataset is divided at 0.01 km^2 and 0.1 km^2, which divides the hotspot sites into groups such that 33% of the locations fall in class (a), 44% in class (b), and 36% in class (c).

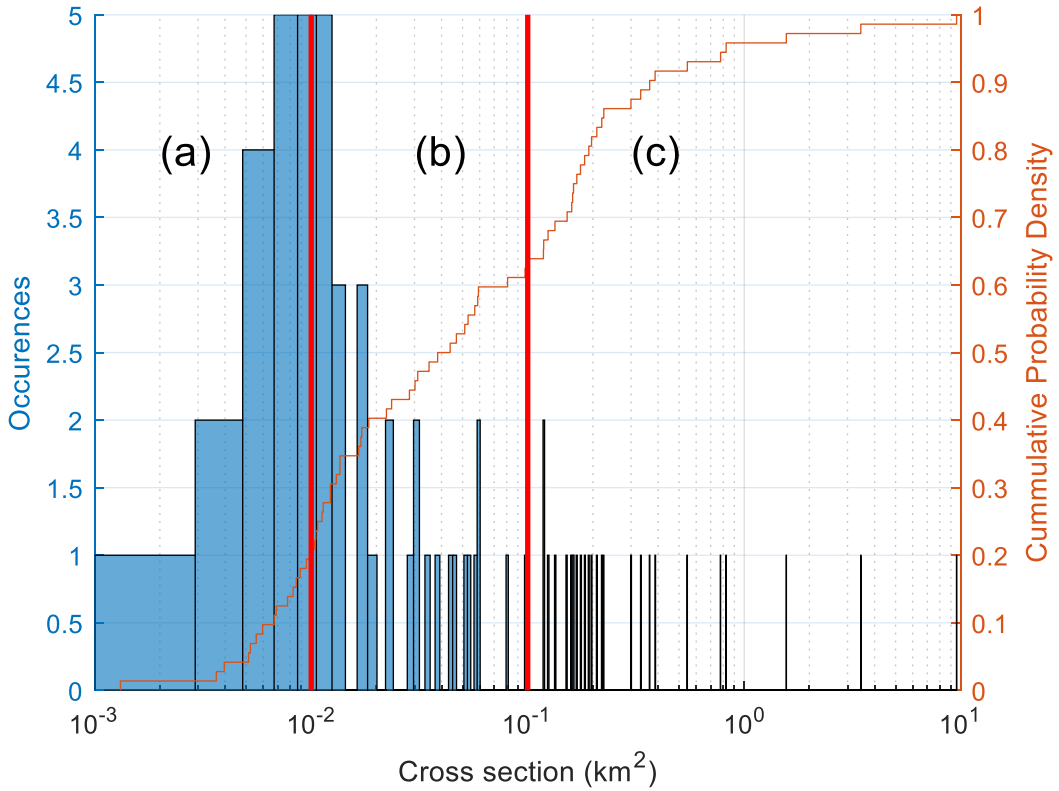

Figure 34 Secondary parameter classification scheme, presented on a probability density function of cross-section area (on log-axis) for all the hotspot locations around the US coast from national tidal resource assessment report (Haas et al., 2011).

Finally, Table 8 shows the tidal stream classifications defined by power density as a primary parameter and cross-sectional area as the secondary parameter. Hence, the twelve classes of the tidal resource were formed. All the classes have at least one hotspot site associated with each class. All the hotspot locations around the US coast are also delineated

based on these two parameters in Figure 35. In figure 35, the depth is shown as the third variable in the form of the color of the data points, in addition to the primary and secondary parameter for resource classification, the depth is also an essential metric which dictates the scale of the tidal device that could be deployed at a site. Hence, it is an additional parameter that aides the resource classification.

Table 8 Tidal stream energy resource classifications

Power Class		***I***	***II***	***III***	***IV***
Power Density (kWh/m^2)		$\boldsymbol{P \geq 2}$	$\boldsymbol{1 \leq P < 2}$	$\boldsymbol{0.5 \leq P < 1}$	$\boldsymbol{P < 0.5}$
Mean Velocity (m/s)		$\boldsymbol{V_m \geq 1.3}$	$\boldsymbol{1.05 \leq V_m < 1.3}$	$\boldsymbol{0.8 \leq V_m < 1.05}$	$\boldsymbol{V_m < 0.8}$
(a)	$\boldsymbol{Area \geq 10^{-1} km^2}$	I(a)	II(a)	III(a)	IV(a)
(b)	$\boldsymbol{10^{-2} km^2 \leq Area < 10^{-1} km^2}$	I(b)	II(b)	III(b)	IV(b)
(c)	$\boldsymbol{Area < 10^{-2} km^2}$	I(c)	II(c)	III(c)	IV(c)

In this way, the resource classification system establishes standard design target requirements that ensure the engineering integrity of the tidal industry. It also enables the industry to target the geographical regions of interest for specific extraction technology. Standard tidal turbines can be designed and manufactured for each of the twelve standard tidal resource classes, resulting in streamlining of the design guidelines and hence reduction in manufacturing costs. This system is a very useful tool for decision-makers to

understand the spatial variability of the tidal resource and the limit of the technical power available at a location.

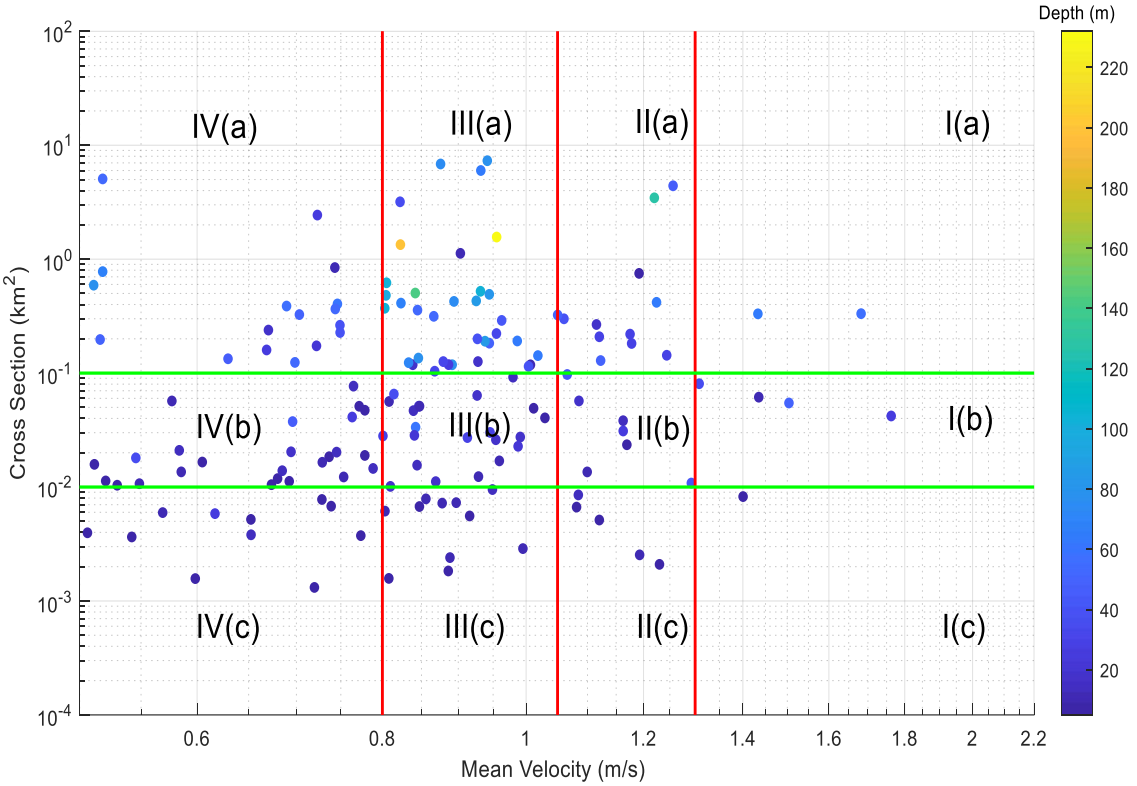

Figure 35 Scatter plot of mean velocity vs x-section for all the hotspot locations around the US coast from national tidal resource assessment report (Haas et al., 2011). The 12 classes of resource were delineated by creating 4 categories of primary parameter and 3 categories of secondary parameter. The red lines divide the data based on primary resource classification parameter and likewise, green lines divide the secondary parameter of resource appraisal.

Based on the final classification scheme, all the national tidal assessment data is classified into the four primary classes and shown on a U.S map in Figure 36. Although most of the coast appears to have velocities less than 0.8 m/s in the figure, there are numerous sites along the coast which have higher velocities. To visualize those high-velocity sites, the tidal mean current data for the top four hotspots, as identified by Kilcher

et al., 2016, are plotted in Figures 37-40. Tacoma Narrows (Figure 37) is considered the best choice for a tidal stream project based on the long- term scoring model by Kilcher et al., 2016. With an available power density of 2 kW/m^2, the Tacoma Narrows site falls under class I. The site also has an average depth of 33 meters. Figure 38 shows the resource mapping of Western Passage, which is one of the highest density sites in the rankings with an average power density of 3 kW/m^2 and an average depth of 35 m across the channel. The next two ranks in the hotspot chart are Rosario Strait and Cook Inlet. They both have relatively more significant markets; hence they make it to top of the ranking table as the viable sites with available power densities of 2.2 kW/m2 and 2.1 kW/m2 respectively and an average depth of 50 m and 41 m respectively. All the four sites mapped here fall under class I and have an average depth of more than 30 meters. Out of the 38 sites ranked by Kilcher et al., 2016 as hotspots, eight falls under class I, 15 in class II, and the rest in class III.

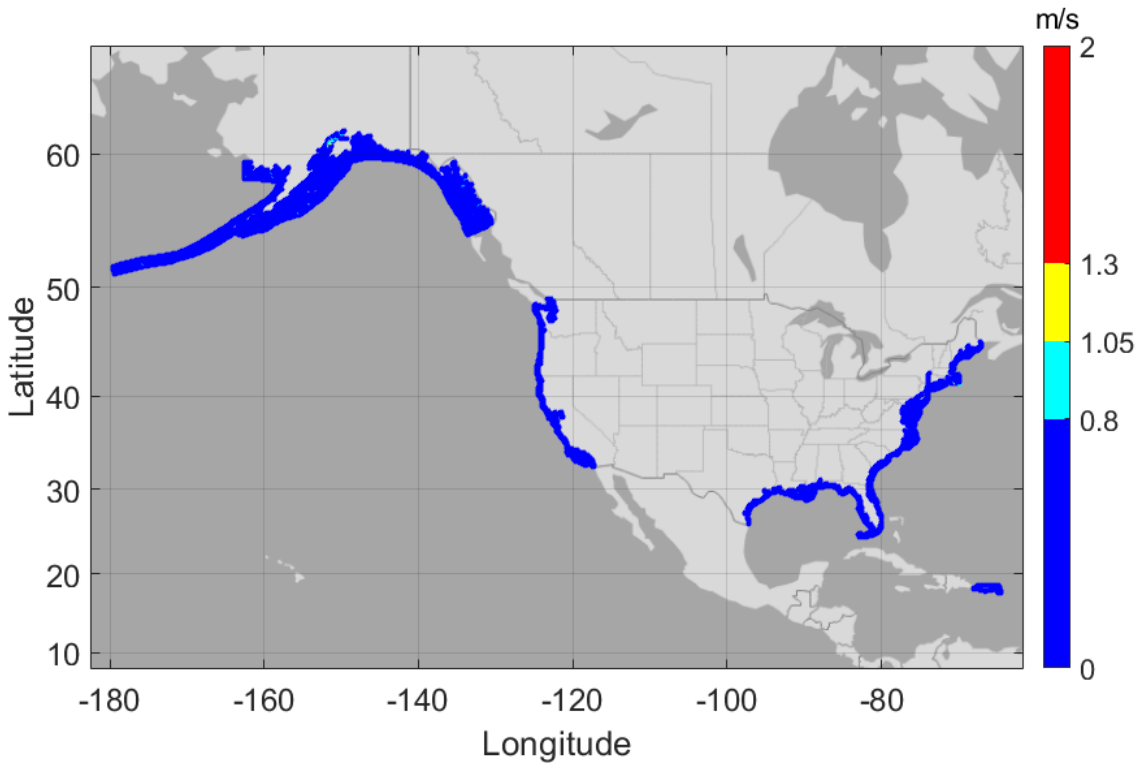

Figure 36 Tidal stream mean currents across the U.S coast, color-coded by their classes. Red, Yellow, Cyan, Blue colors represent Classes I-IV, respectively.

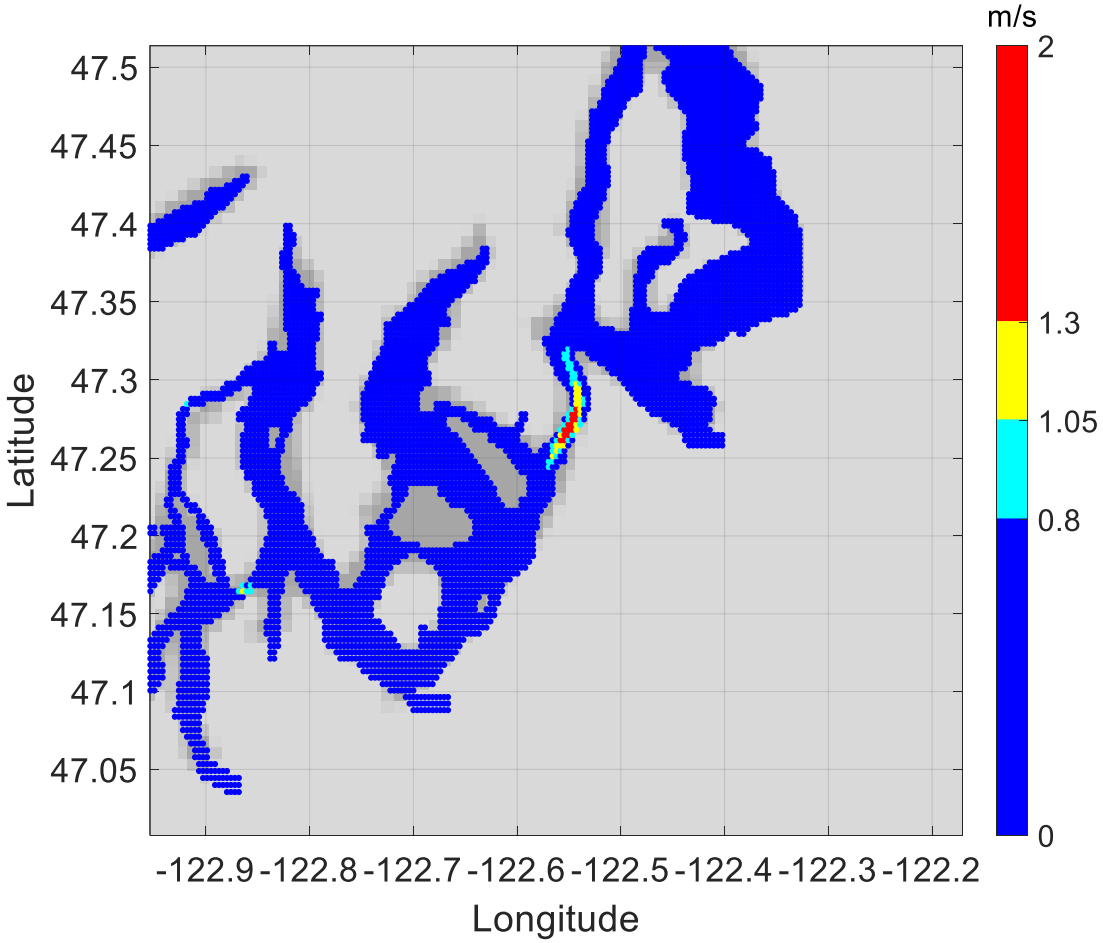

Figure 37 Tidal stream mean currents across Tacoma Narrows (47.28 N, 122.55 W), color-coded by their classes. It is the second ranked tidal energy site, as per the long-term scoring model by Kilcher et al., 2016. Red, Yellow, Cyan, Blue colors represent Classes I-IV, respectively.

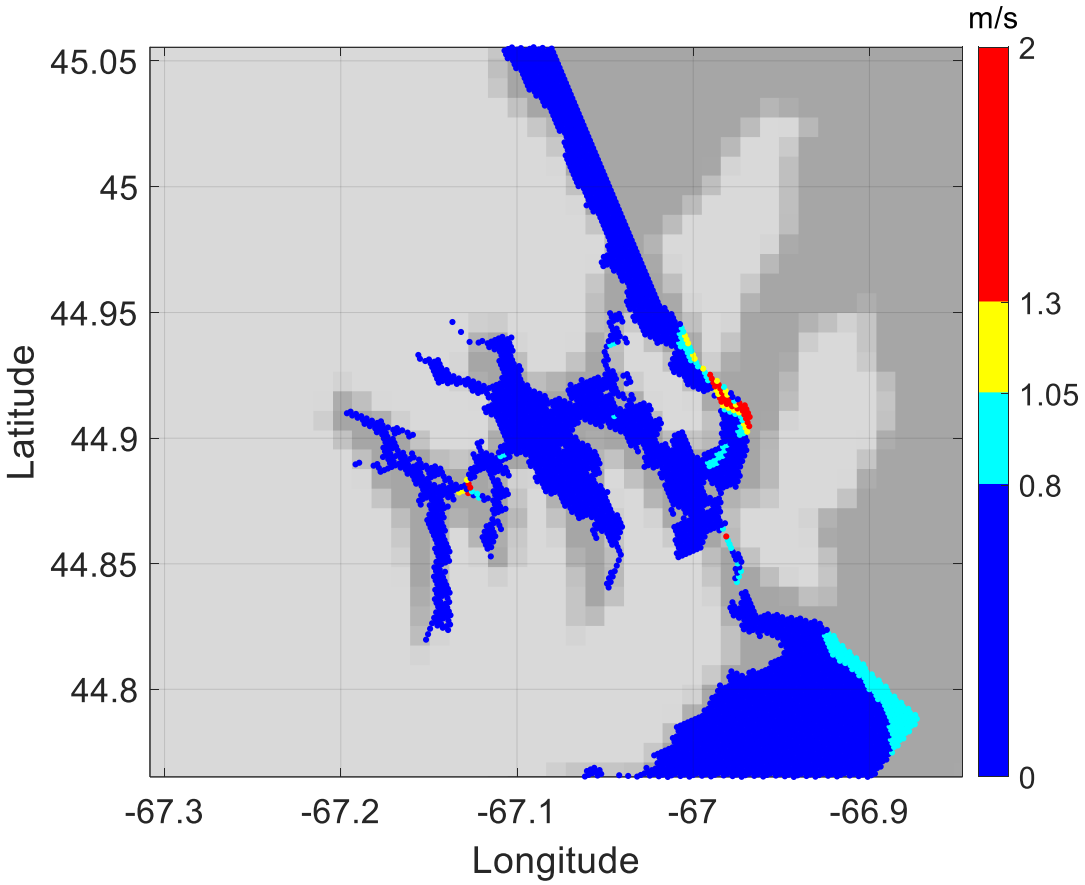

Figure 38 Tidal stream mean currents across Western Passage (44.92 N, 66.99 W), color-coded by their classes. It is ranked third in hotspot ranking, as per the long-term scoring model by Kilcher et al., 2016. Red, Yellow, Cyan, Blue colors represent Classes I-IV, respectively.

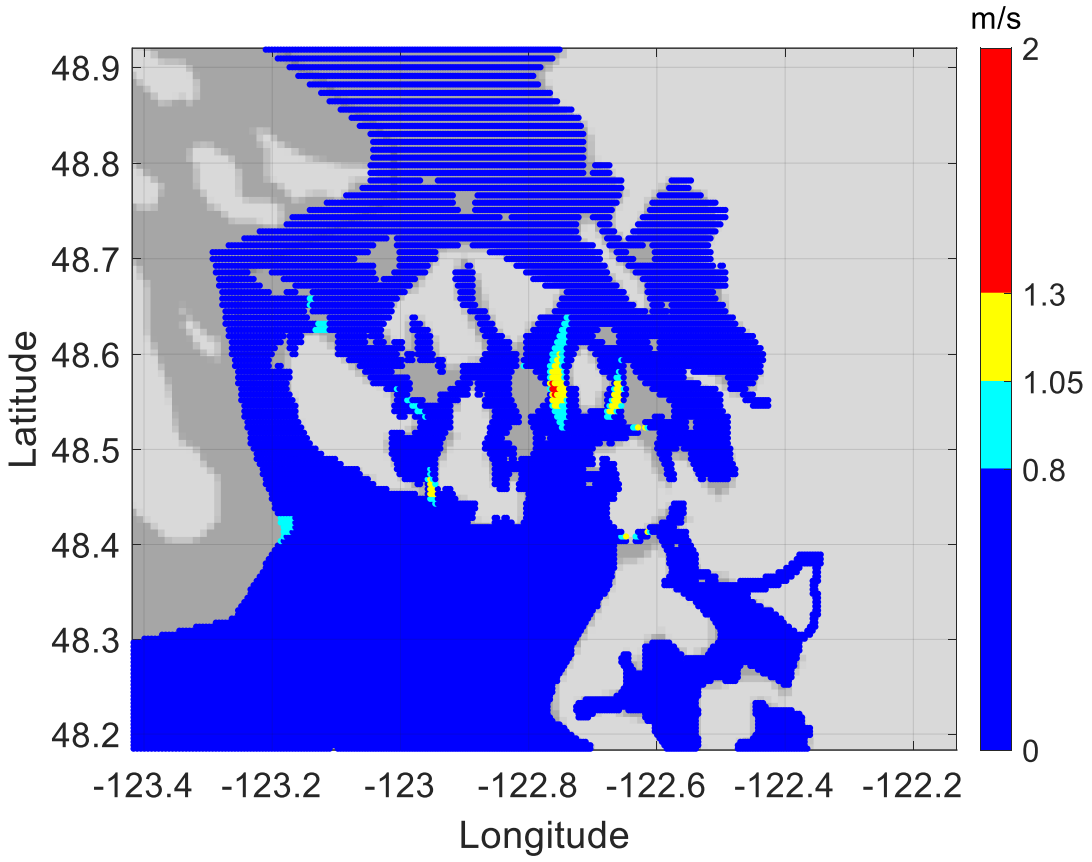

Figure 39 Tidal stream mean currents across Rosario Strait (48.58 N, 122.75 W), color-coded by their classes. It is ranked three tidal energy sites as per the long-term scoring model by Kilcher et al., 2016. Red, Yellow, Cyan, Blue colors represent Classes I-IV, respectively.

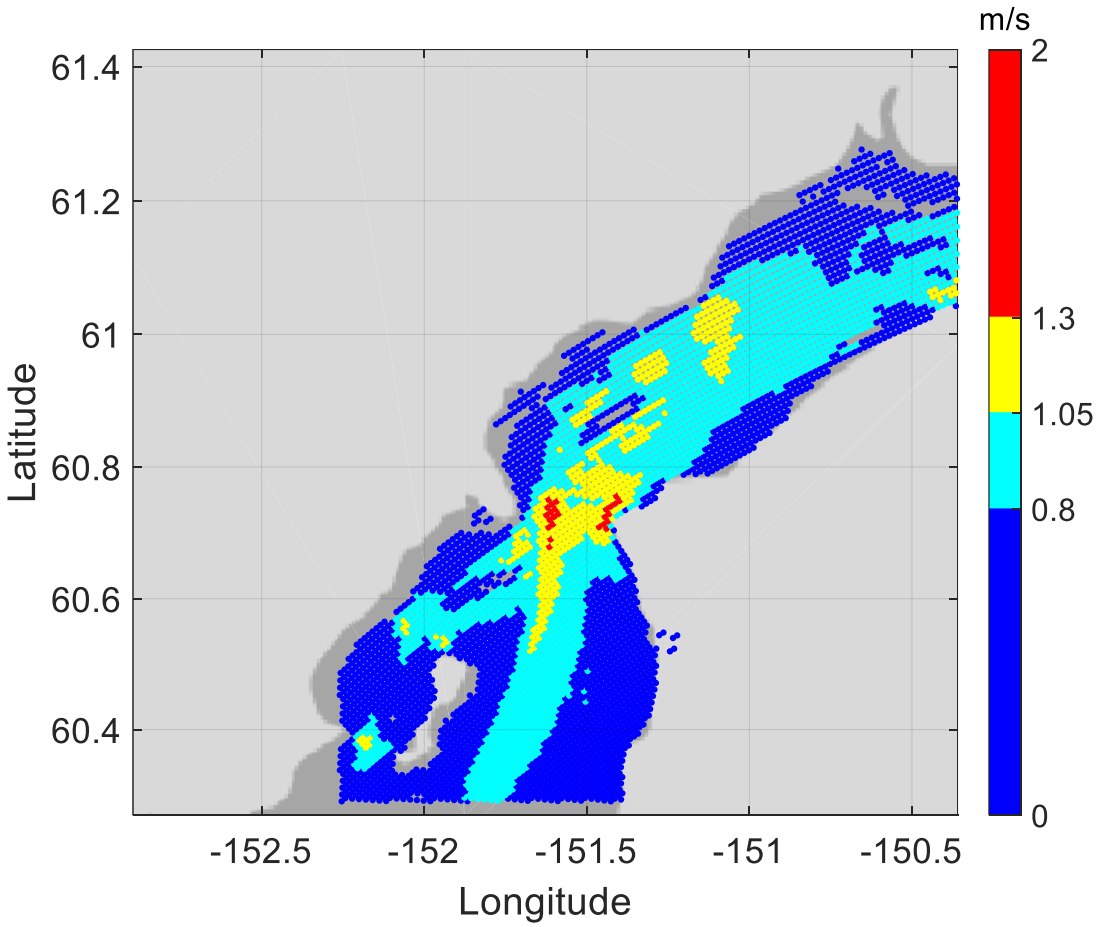

Figure 40 Tidal stream mean currents across Cook Inlet (60.79 N, 151.26 W), color-coded by their classes. It is ranked four tidal energy sites, as per the long-term scoring model by Kilcher et al., 2016. Red, Yellow, Cyan, Blue colors represent Classes I-IV, respectively.

CHAPTER 4. CONCLUSIONS

Tidal energy is still a fledgling sector with excellent potential for renewable energy in the United States. Its predictability gives it an advantage over other non-conventional sources such as wind, solar, and ocean wave energy. In the development of tidal energy projects, it is crucial to appraise the value of the resource to access the viability of a project. Also, to compare the sites for the relative advantage of installing the project at a particular location, a resource classification scheme would play a crucial role in making decisions.

In this study, the goal was to develop a tidal resource classification scheme for the U.S. to reap similar benefits as the wind industry. Classification parameters were calculated from the reconstructed time series of water elevation and velocity across the U.S. coast based on the national tidal assessment database. The reconstruction method was verified by comparing the re-generated time-series against the observed data from NOAA. From the annual tidal data of nine years, the year 2015 was selected for further analyses, based on the highest values of parameter due to nodal precessions. As with the wind energy sector, power density is considered as the primary classification parameter, and various classifying schemes were evaluated to finally arrive at the final classifying plan laid out in Table 7. Also, several relationships were evaluated between the mean velocity and design parameters like maximum annual velocity, 1% exceedance velocity, mean power density.

Although the primary parameter appraised the tidal resource, in order to gauge the scale of extractable energy, several physical parameters were evaluated, such as depth, width, surface area, cross-sectional area, to be considered for secondary parametrization. It was observed that the cross-sectional area of a stream is a suitable proxy for the

maximum theoretical power extractable from a site, and hence it is a convenient way to access the amount of harnessable energy by bypassing the tedious calculations for maximum theoretical power using G&C analysis. The secondary parameter was sub-classified into three classes. Finally, based on the four classes of primary parameter and three classes of the secondary parameter, a tidal resource classification scheme was developed to classify all the locations around the U.S. into twelve categories, based on the availability of the tidal resource (Table 8), needed to optimize tidal energy harnessing devices and arrays, which are very specific to the unique conditions of the physical environment.

The tidal resource classification system developed in this study would undergo review, feedback, and refinement by the MHK community in the US, including the Water Power Technologies Office of the US Department of Energy, the NHA-MEC Resource Assessment Subcommittee and the US Technical Advisory Group (TAG) to IEC TC 114. As for wind, it is expected that a tidal power classification system will go through further refinement as commercial projects are constructed, and operational experience is gained (Neary et al., 2019).

4.1 Future Work

This classification system work could be augmented by developing the tidal device classification system as described by Neary et al. 2019 and Bittencourt 2014, which would categorize the range of conditions in which the devices would operate. This system would also support the manufacturing of devices and streamline the early development and planning of MHK projects.

One potentially viable tidal condition (device) classification system, which is modeled after the IEC wind power classification scheme, is illustrated in Table 9. Main parameter, reference tidal current speed, V_{ref}, would be based on max, 3-min avg current for extreme design load case (DLC). Subclass parameter, turbulence intensity values would be the same as those used to define wind power classes and are likely reasonable, given both wind, and tidal currents are boundary layer flows, and wind shear driven subsurface currents are negligible. Turbulence intensity, as for wind, would characterize unsteady loads under normal and extreme conditions.

Table 9 Tidal power device classification scheme, strawman. Here, A, B, C, represent high ($0.15 < \boldsymbol{I_{ref}} \leq 0.2$), moderate ($0.1< \boldsymbol{I_{ref}} \leq 0.15$) and low value ($\boldsymbol{I_{ref}} \leq 0.10$) of $\boldsymbol{I_{ref}}$ respectively (Neary et al., 2019).

TEC Class		**I**	**II**	**III**	**S**
V_{ref} [m/s]		3.5	2.5	1.5	Values specified by designer
A	I_{ref} [-] @1.5 m/s	0.20			
B		0.15			
C		0.10			

APPENDIX A. HOTSPOT LOCATIONS

Table 10 The hotspot locations considered for computing all the secondary classification parameters from Haas et al., 2011.

State	Hotspot	Latitude	Longitude	Surface Area (km^2)	Mean Depth (m)	Kinetic Power Density (W/m^2)
ME	CoobscookBay	44.891	-67.107	1	14	574
ME	LubecChannel	44.853	-66.977	1	7	891
ME	GrandMananChannel	44.8	-66.892	21	79	768
ME	WesternPaasage	44.911	-66.977	7	43	7366
ME	Knubblebay	43.882	-69.731	1	11	730
ME	HockmockBay	43.902	-69.737	1	7	1747
ME	HockmockBay	43.912	-69.718	1	6	567
ME	KennebeckRiver	43.93	-69.81	1	7	552
ME	KennebeckRiver	43.969	-69.825	1	8	528
ME/NH	PiscataquaRiver	43.073	-70.728	2	13	2823
ME/NH	PiscataquaRiver	43.092	-70.775	1	12	2633
ME/NH	PiscataquaRiver	43.113	-70.807	1	9	1239
MA	NantucketSound	41.197	-69.902	398	16	7328
MA	NantucketSound	41.345	-70.396	202	10	4844
MA	VineyardSound	41.499	-70.647	137	19	3344
MA	VineyardSound	41.362	-70.854	2	15	603
NY	BlockIslandSound	41.229	-72.061	7	38	740
NY	BlockIslandSound	41.167	-72.21	2	21	610
NY	BlockIslandSound	41.075	-71.845	4	12	530
NY	EastRive	40.79	-73.935	1	5	547
NY	EastRive	40.775	-73.937	1	6	1546
NY	EastRive	40.706	-73.979	1	11	768
NJ	DelawareBay	38.921	-74.963	11	9	913
NC	CapeHatteras	35.185	-75.762	1	8	1378
NC	PortsmouthIsland	35.068	-76.016	3	7	911
SC	CooperRiver	32.88	-79.961	1	7	830
SC	NorthEdistoRiver	32.576	-80.2	7	12	1008
SC	CoosawRiver	32.492	-80.49	12	10	566
GA	OgeecheeRiver	31.856	-81.118	1	7	834
GA	AltamahaRiver	31.319	-81.309	1	6	511
GA	SatillRiver	30.97	-81.505	1	7	606
GA/FL	StMarysRiver	30.707	-81.445	5	12	798

Table 10 Continued

GA/FL	StMarysRiver	30.721	-81.508	1	6	705
FL	FloridaKeys	24.692	-81.143	3	6	992
FL	FloridaKeys	24.681	-81.168	1	6	643
FL	FloridaKeys	24.574	-81.839	10	7	904
FL	FloridaKeys	24.556	-82.056	29	6	538
FL	PortBocaGrande	26.716	-82.251	1	10	1140
FL	StVincrntisland	29.625	-85.101	1	8	625
CA	GoldenGate	37.822	-122.471	1	50	750
CA	CarquinezStrait	38.036	-122.158	12	19	914
CA	HumboltBayEntrance	40.757	-124.231	1	9	941
OR	CoosBayEntrance	43.353	-124.339	1	8	2480
WA	ColumbiaRiver	46.254	-124.026	35	11	1751
WA	ColumbiaRiver	46.253	-123.563	2	10	689
WA	GraysHarbor	46.917	-124.117	11	8	576
WA	HaroStrait	48.495	-123.154	15	232	625
WA	HaroStrait	48.587	-123.218	15	199	503
WA	SpiedenChannel	48.63	-123.126	5	43	1893
WA	PresidentChannel	48.656	-123.139	4	39	1227
WA	PresidentChannel	48.679	-122.999	4	129	528
WA	SanJuanChannel	48.547	-122.978	7	62	1030
WA	MiddleChannel	48.459	-122.949	8	60	2380
WA	BoundaryPass	48.735	-123.061	8	163	620
WA	RosarioStrait	48.594	-122.755	45	53	3349
WA	BellinghamChannel	48.556	-122.658	17	27	3077
WA	GuemesChannel	48.523	-122.621	2	7	1777
WA	DeceptionPass	48.407	-122.627	2	6	1058
WA	AdmiraltyInlet	48.162	-122.737	54	62	907
WA	PugetSound	47.591	-122.559	2	11	2568
WA	TacomaNarrows	47.268	-122.544	13	39	5602
WA	DanaPaasage	47.164	-122.862	3	13	1851
AK	BristolBay	58.604	-162.268	160	28	5000
AK	BristolBay	58.532	-160.923	11	11	654
AK	BristolBay	58.442	-158.693	304	12	957
AK	NushagakBay	58.975	-158.519	122	8	2811
AK	HagueChannel	55.908	-160.574	1	17	564
AK	HerendeenBayEntrance	55.892	-160.793	10	19	1564
AK	MoffetLagoonInlet	55.446	-162.587	1	7	845
AK	IzembekLagoon	55.328	-162.896	1	7	539
AK	IzembekLagoon	55.248	-162.981	1	6	1606
AK	BechevinBay	55.048	-163.45	4	6	2252

Table 10 Continued

AK	FalsePass	54.827	-163.384	5	35	1619
AK	UnimakPass	54.333	-164.824	132	57	830
AK	UgamakStrait	54.168	-164.914	63	48	1341
AK	DerbinStrait	54.092	-165.235	23	54	2348
AK	AvatanakStrait	54.108	-165.478	73	73	911
AK	AkutanBay	54.129	-165.649	4	26	3365
AK	AkutanPass	54.025	-166.074	50	49	2870
AK	UnalgaPass	53.948	-166.21	25	64	3751
AK	UmnkPass	53.322	-167.893	97	56	2144
AK	SamalgaPass	52.808	-169.122	8	13	4102
AK	SamalgaPass	52.765	-169.346	138	103	1718
AK	SamalgaPass	52.757	-169.686	66	140	794
AK	IslandsofFourMountains	52.862	-169.998	7	53	2505
AK	SeguamPass	52.247	-172.673	52	129	800
AK	SeguamPass	52.132	-172.826	128	85	538
AK	AtkaIsland	52.121	-174.065	41	36	3444
AK	FenimorePass	51.998	-175.388	4	52	2147
AK	FenimorePass	51.979	-175.477	28	16	1554
AK	FenimorePass	51.974	-175.532	3	50	2410
AK	FenimorePass	51.961	-175.649	1	20	1304
AK	ChugulIsland	51.937	-175.755	9	47	1677
AK	ChugulIsland	51.961	-175.866	9	48	1600
AK	IgitkinIsland	51.968	-175.974	9	59	1110
AK	UnmakIsland	51.857	-176.066	1	22	1155
AK	LittleTanagaStrait	51.818	-176.254	6	43	2276
AK	KagalaskaStrait	51.79	-176.414	1	18	758
AK	AdakStrait	51.816	-176.982	63	63	807
AK	KanagaPass	51.723	-177.748	36	29	889
AK	DelarofIslands	51.677	-178.19	83	78	764
AK	DelarofIslands	51.55	-178.467	54	64	649
AK	DelarofIslands	51.564	-178.716	8	11	537
AK	DelarofIslands	51.586	-178.928	31	66	1053
AK	ChirikofIsland	55.964	-155.45	198	31	597
AK	TugidakIsland	56.294	-154.872	284	26	681
AK	SitkinakIsland	56.512	-154.383	13	8	3104
AK	AiaktalikIsland	56.639	-154.072	79	28	2497
AK	AiaktalikIsland	56.738	-154.053	23	16	2038
AK	MoserBay	57.038	-154.115	3	7	1874
AK	KopreanofStrait	57.934	-152.84	17	29	5454
AK	KopreanofStrait	57.987	-152.795	10	14	4636

Table 10 Continued

AK	ShuyakStrait	58.466	-152.496	2	15	1007
AK	StevensonEntrance	58.647	-152.292	33	102	895
AK	StevensonEntrance	58.663	-152.525	7	39	779
AK	BarrenIslands	58.939	-152.127	15	73	686
AK	BarrenIslands	58.855	-152.345	9	78	571
AK	ChugachIsland	59.091	-151.777	34	54	587
AK	ChugachIsland	59.12	-151.875	19	64	528
AK	ChugachIsland	59.148	-151.74	15	26	1466
AK	ChugachIsland	59.163	-151.531	13	34	916
AK	ChugachIsland	59.082	-151.433	20	47	852
AK	CookInlet	60.676	-151.58	5285	34	5344
AK	TurnagainArm	60.978	-149.825	8	9	3199
AK	TurnagainArm	60.982	-149.702	5	5	657
AK	TurnagainArm	60.998	-149.729	2	5	558
AK	KnikArm	61.385	-149.809	4	6	1993
AK	KnikArm	61.396	-149.77	2	5	742
AK	KnikArm	61.41	-149.734	2	5	749
AK	KnikArm	61.428	-149.709	3	6	597
AK	KnikArm	61.371	-149.726	3	6	1048
AK	ShelikofStrait	58.239	-151.752	15	24	524
AK	MontagueStrait	59.767	-147.966	29	26	691
AK	IcyStrait	58.353	-135.994	274	94	8781
AK	CrossSound	58.223	-136.356	3	72	976
AK	CrossSound	58.225	-136.302	3	79	503
AK	CrossSound	58.256	-136.372	1	46	945
AK	CrossSound	58.288	-135.819	9	84	513
AK	AdamsInlet	58.863	-135.979	4	9	1426
AK	PerilStrait	57.455	-135.549	1	7	3285
AK	PerilStrait	57.371	-135.695	2	24	892
AK	Takuinlet	58.384	-134.032	4	10	864
AK	SeymourCanal	57.922	-134.156	1	14	770
AK	SeymourCanal	57.93	-134.276	1	5	976
AK	SummerStrait	56.369	-133.658	11	67	1474
AK	SummerStrait	56.437	-133.19	6	15	801
AK	SummerStrait	56.441	-133.028	4	101	529
AK	DuncanCanal	56.54	-133.088	1	37	604
AK	KashevarofPassage	56.233	-133.043	6	27	1039
AK	KashevarofPassage	56.269	-132.948	7	80	744
AK	MearesPassage	55.259	-133.109	1	14	1692

Table 11 Additional hotspot locations considered for computing all the classification parameters, from Kilcher et al., 2016.

Latitude	Longitude
41.35	-70.37
43.08	-70.75
48.54	-122.98
57.79	-152.41
37.82	-122.48
41.22	-72.07
30.71	-81.45
47.59	-122.56
44.88	-67.13
48.66	-123.17
41.52	-70.68
24.7	-81.15
41.44	-70.84
59.04	-158.46
24.65	-81.29
30.98	-81.52
35.07	-76.02
55.48	-133.15
26.71	-82.26

REFERENCES

Ahn, S., Haas, K.A., and Neary, V.S., 2019. Wave energy resource classification system for US coastal waters. Renewable and Sustainable Energy Reviews, 104, pp.54-68.

Alderney, 2020, https://tethys.pnnl.gov/project-sites/openhydro-alderney (Accessed April 24, 2020).

Bedard, R, Previsic, M, Siddiqui, O, Hagerman, G, and Robinson, M., 2006. North American Tidal in Stream Energy Conversion Feasibility Demonstration Project. EPRI TP-04-NA. Electric Power Research Institute.

Bergillos, R.J., Rodriguez-Delgado, C., and Iglesias, G., 2020. Management of Coastal Erosion Under Climate Change Through Wave Farms. In Ocean Energy and Coastal Protection (pp. 59-73). Springer, Cham.

Bittencourt, C., K. Argyriadis, M. Steinigar, 2014, "Type-classification for horizontal axis tidal turbine (HATT)—An important step towards commercialisation," Proc. of the Intnl. Conf. of Ocean, Offshore and Arctic Engineering (OMAE).

Board, O.S., National Research Council and Marine and Hydrokinetic Energy Technology Assessment Committee, 2013. An evaluation of the US Department of Energy's marine and hydrokinetic resource assessments. National Academies Press.

Clarence Strait, 2020, https://tethys.pnnl.gov/project-sites/clarence-strait-tidal-energy-project (Accessed April 24, 2020).

Defne, Z., Haas, K.A., Fritz, H.M., Jiang, L., French, S.P., Shi, X., Smith, B.T., Neary, V.S., and Stewart, K.M., 2012. National geodatabase of tidal stream power resource in USA. *Renewable and Sustainable Energy Reviews*, *16*(5), pp.3326-3338.

Energy Efficiency and Renewable Energy (EE&RE), https://www.energy.gov/eere/-water/marine-and-hydrokinetic-resource-assessment-andcharacterization-#tidalstreams (Accessed December 15, 2019).

EIA's Annual Energy Outlook, https://www.eia.gov/outlooks/aeo/ (Accessed December 15, 2019).

Eurostat, E.C., 2013. Energy, transport, and environment indicators-2013 edition. Publications Office of the European Union, Luxembourg.

FERC, 2019. https://www.ferc.gov/industries/hydropower/geninfo/licensing/hydro-kinetics.asp

Froberg, E., 2006. Current Power Resource Assessment. Uppsala University, Uppsala.

Garrett, C., and Cummins, P., 2005. The power potential of tidal currents in channels. Proceedings of the royal society A: mathematical, physical and engineering sciences, 461(2060), pp.2563-2572.

Haas, K.A., and Muscalus, A.C., 2018. Marine Hydrokinetic Energy: Tidal Streams. Advances in Coastal Hydraulics, p.457.

Haas, K.A., Fritz, H.M., French, S.P., Smith, B.T., and Neary, V., 2011. Assessment of energy production potential from tidal streams in the United States. Georgia Tech Research Corporation, Atlanta, GA (United States).

Haas, K.A., Singh, S., and Neary, V.S., 2019, December. Development of a Tidal Energy Resource Classification System. In AGU Fall Meeting 2019. AGU.

Haigh, I.D., Eliot, M., and Pattiaratchi, C., 2011. Global influences of the 18.61-year nodal cycle and 8.85 year cycle of lunar perigee on high tidal levels. Journal of Geophysical Research: Oceans, 116(C6).

Hooper, T., and Austen, M., 2013. Tidal barrages in the UK: Ecological and social impacts, potential mitigation, and tools to support barrage planning. Renewable and Sustainable Energy Reviews, 23, pp.289-298.

HydroReview, 2020, https://www.hydroreview.com/2011/01/14/tidal-current-power/#gref (Accessed April 24, 2020).

Kilcher, L., Thresher, R., and Tinnesand, H., 2016. Marine Hydrokinetic Energy Site Identification and Ranking Methodology Part II: Tidal Energy (No. NREL/TP-

5000-66079). National Renewable Energy Lab. (NREL), Golden, CO (United States).

Jacobson, P.T., Ravens, T.M., Cunningham, K.W., and Scott, G., 2012. Assessment and Mapping of the Riverine Hydrokinetic Resource in the Continental United States (No. DOE/EE/0002662-1). Electric Power Research Institute.

Jenne, D.S., Yu, Y.H., and Neary, V., 2015. Levelized cost of energy analysis of marine and hydrokinetic reference models (No. NREL/CP-5000-64013). National Renewable Energy Lab (NREL), Golden, CO (United States).

LLC, O.M., 2014. Cobscook Bay Tidal Energy Project: 2013 Environmental Monitoring Report.

Manwell, J.F., McGowan, J.G., and Rogers, A.L., 2010. Wind energy explained: theory, design, and application. John Wiley & Sons.

MeyGen, 2020, https://tethys.pnnl.gov/project-sites/meygen-tidal-energy-project-phase-i (Accessed April 24, 2020).

NASA, 2019, https://climate.nasa.gov/effects/ (Accessed December 20, 2019).

Neary, V.S., Coe, R.G., Cruz, J., Haas, K., Bacelli, G., Debruyne, Y., Ahn, S., and Nevarez, V., 2018. Classification systems for wave energy resources and WEC technologies. International Marine Energy Journal, 1(2 (Nov)), pp.71-79.

Neary, V.S., Haas, K. A., J. Colby, “Marine Energy Classification Systems: Tools for resource assessment and design,” European Wave and Tidal Energy Conference (EWTEC), Naples, Italy, 2019.

NOAA, 2019, https://tidesandcurrents.noaa.gov/stations.html?type=Water+Levels (Accessed December 20, 2019).

Pawlowicz, R., Beardsley, B., and Lentz, S., 2002. Classical tidal harmonic analysis, including error, estimates in MATLAB using T_TIDE. Computers & Geosciences, 28(8), pp.929-937. (https://www.eoas.ubc.ca/~rich/)

Power, V., 2011. Roosevelt Island Tidal Energy (RITE) environmental assessment project: final report. NYSERDA report, pp.11-04.

Race Rocks, 2020, https://tethys.pnnl.gov/publications/summary-report-environmental-monitoring-related-pearson-college-encana-clean-current (Accessed April 24, 2020).

Roadmap, O.E.S., 2016, November. Building Ocean Energy for Europe. In Ocean Energy Forum (Vol. 8).

Schlütter, F., Petersen, O.S. and Nyborg, L., 2015. Resource mapping of wave energy production in Europe. In Proceedings of the 11th European wave and tidal energy conference, 10B4-3.

Segura, E., Morales, R., and Somolinos, J.A., 2018. A strategic analysis of tidal current energy conversion systems in the European Union. Applied energy, 212, pp.527-551.

Shetland Tiday Array, 2020, https://tethys.pnnl.gov/project-sites/nova-innovation-shetland-tiday-array-bluemull-sound (Accessed April 24, 2020).

Strangford Narrows, 2020, https://simecatlantis.com/projects/strangford-narrows/ (Accessed April 24, 2020).

Tethys, https://tethys.pnnl.gov/project-sites/admiralty-inlet-pilot-tidal-project (Accessed December 20, 2019).

U.S. EIA, 2019, https://www.eia.gov/energyexplained/hydropower/tidal-power.php (Accessed December 20, 2019).

Verdant Power, 2019, https://www.verdantpower.com/riteproject (Accessed December 20, 2019).

Water Power Program, 2019, Overview of WPTO & the Marine and Hydrokinetics (MHK) Program, https://www.energy.gov/sites/prod/files/2019/12/f69/10.8.19_01_MHK%20Program%20Overview.pdf (Accessed December 5, 2019).

Yang, X. and Haas, K.A., 2015. Improving assessments of tidal power potential using grid refinement in the Coupled Ocean-Atmosphere-Wave-Sediment Transport model. Journal of Renewable and Sustainable Energy, 7(4), p.043107.

Yang, X., Haas, K.A., Fritz, H.M., French, S.P., Shi, X., Neary, V.S., and Gunawan, B., 2015. National geodatabase of ocean current power resource in USA. Renewable and Sustainable Energy Reviews, 44, pp.496-507.

U.S. Department of Energy (DOE), Water Power Technologies Office (WPTO) Overview of WPTO & the Marine and MHK Program, https://www.energy.gov/sites/prod/files/2019/12/f69/10.8.19_01_MHK%20Program%20Overview.pdf